

# Single-walled carbon nanotubes: the Bloch theory, reciprocal tubes, and a tight-binding approximation

Yuri A. Antipov\*

*Department of Mathematics, Louisiana State University, Baton Rouge LA 70803*

(Dated: December 8, 2025)

The electronic structure of a graphene sheet is altered when it is rolled up to form a single-walled carbon nanotube (SWCNT), and the curvature effects for small radius nanotubes become significant. In the paper, an analogue of the Bloch theory of crystals with translational symmetry to armchair, zigzag, and chiral SWCNTs, cylindrical lattices with rotation-translational symmetry, is proposed. It is based on the use of cylindrical coordinates, three-dimensional characteristic vectors of the lattice, a reciprocal tube, and rotation-translation transformations in the real and reciprocal 3d spaces. The Brillouin zone on the reciprocal tube and the domain of the wave-vector are determined. An analogue of the Bloch theorem for SWCNTs is stated and proved. A tight-binding approximation scheme for orbitals orthogonal to the nanotube surface is described, and the Hamiltonian and overlap matrices associated with the first and second nearest-neighbor tight-binding approximations are derived.

## I. INTRODUCTION

Although carbon nanotubes had been known since the middle of the last century, the active systematic study of electronic, optical and mechanical properties of nanotubes was initiated by the 1991 Iijima's report [1] that described high-resolution electron micrographs of helicon carbon microtubes with the thinnest needle observed having 2.2 nm in diameter. It was pointed out that the helical structure of the needles was entirely different from the screw dislocation model of conventional crystals in the sense that the needle crystals had a cylindrical lattice symmetry. One of the most widely applied techniques for describing the electronic structure of SWCNTs is the zone-folding method [2], a modification of the tight-binding approximation approach developed for graphene [3]. A review [4] described theoretical aspects of graphene and summarized the modern methods including the tight-binding approximation technique for analysis of electronic structure of single-layer and double-layer graphene.

Electronic band structure of SWCNTs analyzed by tight-binding approximation [5] revealed the existence of three classes of nanotubes, metallic, semiconducting with narrow band gaps, and semiconducting with moderate band gaps. Tight-binding folding of the 2d energy bands of graphene was applied [6], [7] to calculate the electronic structure of SWCNTs. On the basis of the calculations it was predicted [7] that approximately a third of SWCNTs were a 1d metal, while the others were 1d semiconductors. A similar procedure was implemented [8] to calculate the  $\pi$ -electron states of SWCNTs in magnetic field. The tight-binding approximation and folding the graphene energy bands were also employed [9] for double-walled carbon commensurate and incommensurate nanotubes. It was concluded that due to the symmetry, the interlayer interaction between the layers did not affect

the metallic nature of the constituent. The symmetry properties of chiral SWCNTs, the zone-folding technique, and the irreducible representations of symmetry groups associated with the chiral vector were employed [10], [11] to classify the electronic wave-functions and the phonon modes at the Brillouin zone center.

Comparison [12] of two approaches for electronic structure of SWCNTs, the graphene based tight-binding approximation and the method of pseudopotential local density functional theory (DFT), revealed that for small radius nanotubes in some cases the band gaps computed by the former theory deviated from those obtained by the second approach by more than 50%. Effects of curvature on the electronic structure of metallic SWCNTs were included [13] into the model by introducing a deformation tensor  $D^{curv} = (d_{ij})$ ,  $i, j = 1, 2$ , with the only one nonzero entry  $d_{11}$ , expressed through a transfer integral, the carbon-carbon bond length, and the nanotube radius. To take into account the curvature effects on electronic structure of SWCNTs, another approach, a symmetry-adapted non-orthogonal tight-binding approximation scheme, was applied in [14]. Electron-phonon interaction in an armchair nanotube (5, 5) and zigzag nanotubes (5, 0) and (6, 0) was analyzed in [15]. By using the Fröhlich Hamiltonian it was found that the zone-folding technique described well the tube (5, 5). In the case of the zigzag nanotubes (5, 0) and (6, 0) the large curvature made these tubes metallic with a large density of states at the Fermi energy and led to unusual electron-phonon interactions, with the dominant coupling coming from the out-of-plane phonon modes. A DFT method for the analysis of torsional deformations of structures with helical symmetry was introduced in [16]. This method was recently adapted and numerically tested [17] to the Schrödinger equation in helical coordinates.

The goal of this work was to develop an analogue of the Bloch theory for armchair, zigzag, and chiral cylindrical lattices. The main feature of the method to be proposed is the use of cylindrical coordinates, three-dimensional characteristic vectors of the nanotube and its reciprocal tube, and rotation-translation transformations  $\mathcal{T}_j^{\pm}$  and

---

\* yantipov@lsu.edu

$\tilde{\mathcal{T}}_j^\pm$  in the real and reciprocal 3d spaces. In Sections II, III, and IV, we describe the structure and symmetry properties of an armchair SWCNT  $(n, n)$ , a chiral nanotube  $(n, m)$ ,  $1 \leq m \leq n - 1$ , and a zigzag nanotube  $(n, 0)$ , respectively. We also construct and characterize the associated reciprocal tubes, introduce the rotation-translation transformations and the corresponding space groups in the real and reciprocal spaces, construct the Brillouin zone and describe the domain of the wave-vector.

In Section V, based on the simultaneous use of the rotation-translation transformations applied to the real nanotube and its reciprocal tube we state and prove an analogue of the Bloch theorem for 2d cylindrical quasi-hexagonal lattices with a curved parallelogram of periods. The Bloch theorem [18] for crystals with translational symmetry consists of two parts. In its modern interpretation [19], [20], the first part states that the Bloch states, solutions of the Schrödinger equation  $\mathcal{H}\psi(\mathbf{r}; \mathbf{k}) = \epsilon(\mathbf{k})\psi(\mathbf{r}; \mathbf{k})$ , are quasiperiodic,

$$\psi(\mathbf{r} + \mathbf{R}; \mathbf{k}) = e^{i\mathbf{k}\cdot\mathbf{R}}\psi(\mathbf{r}; \mathbf{k}), \quad (1)$$

where  $\mathbf{R} = n_i \mathbf{a}_i$ ,  $n_i$  are integers, and  $\mathbf{a}_i$  are the lattice vectors. The second part expresses the function  $\psi(\mathbf{r}; \mathbf{k})$  as the product of the phase factor  $e^{i\mathbf{k}\cdot\mathbf{r}}$  and a periodic function  $u(\mathbf{r}; \mathbf{k})$  that is

$$\psi(\mathbf{r}; \mathbf{k}) = e^{i\mathbf{k}\cdot\mathbf{r}}u(\mathbf{r}; \mathbf{k}), \quad u(\mathbf{r} + \mathbf{R}; \mathbf{k}) = u(\mathbf{r}; \mathbf{k}). \quad (2)$$

Analogues of formula (1) for structures with rotation-translational symmetry were presented in [21], [22], [23], [16]. As an analogue of formula (2), the representation  $\psi(\mathbf{r}; \mathbf{k}) = e^{i\mathbf{k}\cdot\mathbf{n}(\mathbf{r})}u(\mathbf{r}; \mathbf{k})$  with  $\mathbf{n}(\mathbf{r})$  and  $u(\mathbf{r}; \mathbf{k})$  being a vector and a periodic function, respectively, was introduced in [23]. However, they did not give a constructive procedure for the determination of the vector  $\mathbf{n}(\mathbf{r})$ , nor did they prove the existence of the vector  $\mathbf{n}(\mathbf{r})$ . In Section V, by making use of the transformations  $\mathcal{T}_j^\pm$  and  $\tilde{\mathcal{T}}_j^\pm$  we prove that first,  $\psi(\mathcal{T}_j^\pm \mathbf{r}; \mathbf{k}) = e^{\pm i j \kappa c_\pm} \psi(\mathbf{r}; \mathbf{k})$ , where  $j = \pm 1, \pm 2, \dots$ ,  $c_\pm$  are explicitly expressed through the integers  $n$  and  $m$ ,  $\kappa \in I$ , and  $I$  is defined from the Brillouin zone, and second,  $\psi(\mathbf{r}; \mathbf{k}) = e^{i\mathbf{k}\cdot\mathbf{r}}u(\mathbf{r}; \mathbf{k})$ , where  $u(\mathbf{r}; \mathbf{k})$  is invariant with respect to the rotation-translation transformations applied simultaneously in the real and reciprocal spaces,

$$u(\mathcal{T}_j^\pm \mathbf{r}; \tilde{\mathcal{T}}_j^\pm \mathbf{k}) = u(\mathbf{r}; \mathbf{k}). \quad (3)$$

We also derive the governing equation for the function  $u(\mathbf{r}; \mathbf{k})$ . In addition, we write a representation of eigenfunctions of the Hamiltonian operator in a SWCNT subject to the cyclic boundary conditions and verify their orthogonality.

In Section VI, we describe a tight-binding approximation scheme for  $2p_z$ -orbitals with  $z$  orthogonal to the nanotube surface, derive the secular equation, and write down the Hamiltonian and overlap matrices associated with the first and second nearest-neighbor tight-binding approximations.

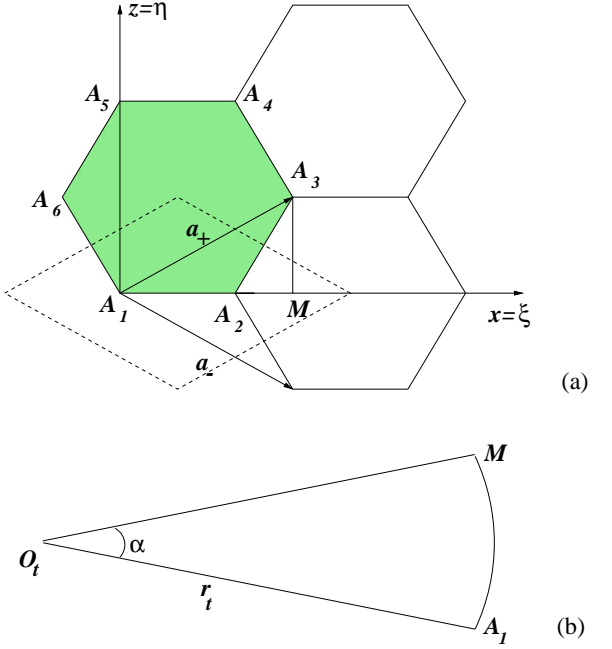


FIG. 1. (a): Hexagonal unit cell. (b): Image of the segment  $A_1M$  on the armchair tube  $\mathcal{A}$ .

## II. ARMCHAIR NANOTUBE AND CONSTRUCTION OF ITS RECIPROCAL TUBE

Let  $(x, y, z)$  and  $(r, \theta, z)$  be Cartesian and cylindrical coordinates, respectively, with the origin at  $O_t$ . In the plane  $\Pi = \{|x| < \infty, y = r_t, |z| < \infty\}$ , introduce Cartesian coordinates centered at  $(0, r_t, 0)$  by the relations  $\xi = x$ ,  $\eta = z$ . Consider an armchair SWCNT,  $\mathcal{A} = \mathcal{A}(n, n)$ , characterized by the chiral vector  $\mathbf{C}_h = (n, n)$  and having  $N$  curved hexagonal cells. The number  $N$  is macroscopically large, and without loss of generality it is a multiple of  $2n$ . Let the radius of the nanotube be  $r_t$ . Assume that the associated unrolled honeycomb lattice (graphene) lies on the plane  $\Pi$  (Fig. 1a) and is characterized by the two vectors

$$\mathbf{a}_+ = \frac{a}{2}\langle\sqrt{3}, 1\rangle, \quad \mathbf{a}_- = \frac{a}{2}\langle\sqrt{3}, -1\rangle, \quad (4)$$

where  $a = 2.46\text{\AA}$  is the lattice constant of graphene. The projection of the vectors  $\mathbf{a}_\pm$  on the  $x$ -axis,  $A_1M$ , when the graphene sheet is rolled up around the  $z$ -axis, becomes a circular arc (Fig. 1b); its length is

$$A_1M = \frac{a\sqrt{3}}{2} = r_t\alpha, \quad (5)$$

where  $\alpha$  is the angle of rotation of the point  $M$  around the  $z$ -axis when the point  $A_1$  ( $x = 0, y = r_t, z = 0$ ) is fixed.

Since the circumference of a cross-section of the carbon armchair nanotube by a plane orthogonal to its axis is the length of the chiral vector,  $|\mathbf{C}_h| = na\sqrt{3}$ , we immediately

find

$$r_t = \frac{na\sqrt{3}}{2\pi}, \quad \alpha = \frac{\pi}{n}. \quad (6)$$

The rolling of the graphene sheet transforms the vectors  $\mathbf{a}_\pm$  into elliptical arcs whose chords have the length

$$a^\circ = a\sqrt{\frac{1}{4} + \frac{3n^2}{\pi^2} \sin^2 \frac{\pi}{2n}}. \quad (7)$$

The values of the dimensionless parameter  $a^\circ/a$  for some  $n$  are listed in Table I. We introduce next two vectors  $\hat{\mathbf{a}}_\pm \in R^3$  which serve for the armchair nanotube  $\mathcal{A}(n, n)$  in the same way as the lattice vectors  $\mathbf{a}_\pm$  work for graphene. They are

$$\hat{\mathbf{a}}_+ = \begin{pmatrix} -r_t \sin \alpha \\ r_t \cos \alpha \\ \frac{a}{2} \end{pmatrix}, \quad \hat{\mathbf{a}}_- = \begin{pmatrix} -r_t \sin \alpha \\ r_t \cos \alpha \\ -\frac{a}{2} \end{pmatrix}. \quad (8)$$

As in the theory of lattices with translational symmetry, we introduce a reciprocal  $\mathbf{k}$ -space,  $\tilde{R}^3$ , and an analogue of the reciprocal lattice, a reciprocal tube,  $\tilde{\mathcal{A}} = \mathcal{A}(n, n)$ . It will be convenient to operate with reciprocal Cartesian and cylindrical coordinates  $(\tilde{x}, \tilde{y}, \tilde{z})$  and  $(\tilde{r}, \theta, \tilde{z})$ , respectively. The reciprocal radius of the cross-section of the tube  $\tilde{\mathcal{A}}$  is  $\tilde{r} = \pi/r_t$ , and the tube is characterized by the reciprocal tube vectors

$$\tilde{\mathbf{b}}_+ = \begin{pmatrix} -\frac{\pi}{r_t} \sin \alpha \\ \frac{\pi}{r_t} \cos \alpha \\ \frac{4\pi}{a} \end{pmatrix}, \quad \tilde{\mathbf{b}}_- = \begin{pmatrix} -\frac{\pi}{r_t} \sin \alpha \\ \frac{\pi}{r_t} \cos \alpha \\ -\frac{4\pi}{a} \end{pmatrix}. \quad (9)$$

Notice that, in contrast to the hexagonal lattice vectors, the real nanotube vectors  $\hat{\mathbf{a}}_\pm$  and reciprocal vectors  $\tilde{\mathbf{b}}_\pm$  are not mutually orthogonal and possess the properties

$$\hat{\mathbf{a}}_\pm \cdot \tilde{\mathbf{b}}_\pm = 3\pi, \quad \hat{\mathbf{a}}_+ \cdot \tilde{\mathbf{b}}_- = \hat{\mathbf{a}}_- \cdot \tilde{\mathbf{b}}_+ = -\pi. \quad (10)$$

As a unit cell of the graphene sheet, we select the interior of the hexagon  $A_1A_2\dots A_6$  complemented by the polygon line  $A_6A_1A_2A_3$  (the vertices  $A_3$  and  $A_6$  and the polygon line  $A_3A_4A_5A_6$  are excluded). As a parallelogram of periods, we choose the parallelogram formed by the vectors  $\mathbf{a}_+$  and  $\mathbf{a}_-$  shifted to the left with the vertices being the centers of the four neighboring hexagons (Fig. 1a). Both polygons, the unit hexagonal cell and the parallelogram of periods, have two carbon atoms,  $A_1$  and  $A_2$ . Call the hexagonal cell chosen and its image on

the nanotube by  $\mathcal{U}_G$  and  $\mathcal{U}_A$ , respectively. Fix a point  $\mathbf{r}$  in the unit cell of the nanotube,

$$\mathbf{r} = \begin{pmatrix} -r_t \sin \theta \\ r_t \cos \theta \\ z \end{pmatrix} \in \mathcal{U}_A, \quad (11)$$

and consider two linear space transformations  $\mathcal{T}_1^+$  and  $\mathcal{T}_1^-$ ,

$$\mathcal{T}_1^\pm \mathbf{r} = \mathcal{R}_1 \mathbf{r} \pm \frac{a}{2} \hat{\mathbf{z}}, \quad \hat{\mathbf{z}} = \begin{pmatrix} 0 \\ 0 \\ 1 \end{pmatrix}, \quad (12)$$

where  $\mathcal{R}_1$  is the transformation of rotation around the  $z$ -axis by angle  $\alpha$  represented by the matrix

$$\mathcal{R}_1 = \begin{pmatrix} \cos \alpha & -\sin \alpha & 0 \\ \sin \alpha & \cos \alpha & 0 \\ 0 & 0 & 1 \end{pmatrix}. \quad (13)$$

The rotation  $\mathcal{R}_j = \mathcal{R}_1 \mathcal{R}_{j-1}$  and rotation-translations  $\mathcal{T}_j^\pm = \mathcal{T}_1^\pm \mathcal{T}_{j-1}^\pm$  have the properties

$$\mathcal{R}_j \mathbf{r} = \begin{pmatrix} -r_t \sin(j\alpha + \theta) \\ r_t \cos(j\alpha + \theta) \\ z \end{pmatrix} \quad (14)$$

and

$$\mathcal{T}_j^\pm \mathbf{r} = \begin{pmatrix} -r_t \sin(j\alpha + \theta) \\ r_t \cos(j\alpha + \theta) \\ z \pm \frac{ja}{2} \end{pmatrix}. \quad (15)$$

It will be convenient to denote the composition of the transformations  $\mathcal{T}_j^+$  and  $\mathcal{T}_s^-$  by

$$\mathcal{M}_{s,j}^{-+} = \mathcal{T}_s^- \mathcal{T}_j^+. \quad (16)$$

The transformations  $\mathcal{M}_{s,j}^{-+}$  map the unit cell  $\mathcal{U}_A^{00} = \mathcal{U}_A$  of the nanotube to the cells  $\mathcal{U}_A^{sj}$  of the infinite armchair nanotube  $\mathcal{A}^\infty(n, n)$ . It becomes evident that

$$\bigcup_{s=0}^{n-1} \bigcup_{j=-\infty}^{\infty} \mathcal{U}_A^{sj} = \mathcal{A}^\infty, \quad (17)$$

and each cell of the nanotube is listed in (17) only once. For a finite armchair nanotube  $\mathcal{A}(n, n)$  having  $N$  curvilinear hexagonal cells,

$$\mathcal{A} = \bigcup_{s=0}^{n-1} \bigcup_{j=-L+s}^{L+s-1} \mathcal{U}_A^{sj}, \quad (18)$$

where  $2nL = N$ , and for all  $s = 0, 1, \dots, n-1$ ,

$$\mathcal{M}_{s,-L+s}^{-+} \mathcal{U}_A^{00} = \mathcal{M}_{s,L+s}^{-+} \mathcal{U}_A^{00}. \quad (19)$$

The transformations  $\mathcal{M}_{s,j}^{-+}$  ( $s = 0, 1, \dots, n-1, j = -L+s, -L+s+1, \dots, L+s$ ) generate a space group say,  $\mathcal{G}_A$ , whose fundamental domain is the unit cell  $\mathcal{U}_A$ .

TABLE I. The parameter  $a^* = a^\circ/a$  for some armchair nanotubes.

$C_h$	(4,4)	(5,5)	(6,6)	(10,10)	(20,20)
$a^*$	0.9809	0.9877	0.9915	0.9969	0.9992

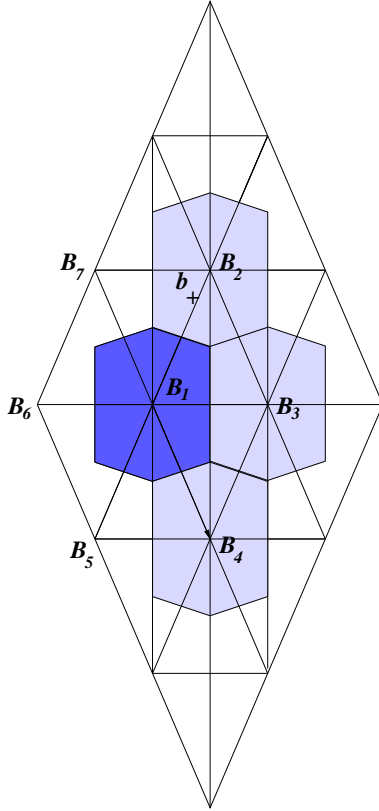


FIG. 2. Unrolled lattice of the tube  $\tilde{A}$ , the reciprocal of an armchair nanotube  $A$ , and the Brillouin zone (the deep blue hexagon).

Consider now the reciprocal tube  $\tilde{A}(n, n)$ . We need to determine its parallelogram of periods, select a unit cell, and introduce an analogue of the transformations  $\mathcal{T}_j^\pm$  in the reciprocal space  $\tilde{R}^3$ . To do so first consider the reciprocal lattice characterized by two vectors  $\mathbf{b}_\pm = \langle b', \pm b'' \rangle$  lying in the reciprocal plane  $\tilde{R}^2$ , with the numbers  $b'$  and  $b''$  to be fixed. Denote the parallelogram (a rhombus) of periods of the reciprocal lattice by  $B_1B_2B_3B_4$  (Fig. 2). The flat reciprocal lattice itself is described by

$$\tilde{\mathbf{r}}(l_1, l_2) = l_1 \mathbf{b}_+ + l_2 \mathbf{b}_-, \quad (20)$$

where  $l_1$  and  $l_2$  are integers. The reciprocal tube is formed by rolling a portion of the reciprocal lattice around the  $\tilde{z}$ -axis. Based on the expressions (9) of the reciprocal tube vectors, we find the vertical diagonal of the rhombus of periods,  $B_2B_4 = \frac{8\pi}{a}$ , and the parameter  $b'' = \frac{4\pi}{a}$ . In virtue of formulas (6) and (9) the radius  $\tilde{r}_t$  of a cross-section of the reciprocal tube orthogonal to its axis is

$$\tilde{r}_t = \frac{\pi}{r_t} = \frac{2\pi^2}{an\sqrt{3}}. \quad (21)$$

Since the circumference of the cross-section is  $2nb' = 2\pi\tilde{r}_t$ , the second diagonal of the rhombus is  $B_1B_3 = 2b' <$

$B_2B_4$ , where

$$b' = \frac{2\pi^3}{an^2\sqrt{3}} < B_2B_4. \quad (22)$$

A unit cell of the reciprocal tube,  $\mathcal{U}_{\tilde{A}}$ , is recovered by rolling the rhombus  $B_1B_2B_3B_4$  around the  $\tilde{z}$ -axis and placing it on the surface of the reciprocal tube. The rhombus sides  $B_1B_2$  and  $B_1B_4$  become elliptic arcs, and their length is

$$\tilde{a} = \frac{2\pi}{a} \sqrt{4 + \frac{\pi^4}{3n^4}}. \quad (23)$$

Choose a point  $\mathbf{k}$  (the wave-vector) on the reciprocal tube  $\tilde{A}$

$$\mathbf{k} = \begin{pmatrix} -\frac{\pi}{r_t} \sin \tau \\ \frac{\pi}{r_t} \cos \tau \\ \kappa \end{pmatrix} \in \tilde{A}, \quad (24)$$

where  $\kappa$  is a real parameter. Next we define the rotation-translation transformations in the reciprocal space by

$$\tilde{\mathcal{T}}_j^\pm \mathbf{k} = \mathcal{R}_j \mathbf{k} \pm \frac{4\pi j}{a} \hat{z} \quad (25)$$

or, equivalently, by

$$\tilde{\mathcal{T}}_j^\pm \mathbf{k} = \begin{pmatrix} -\frac{\pi}{r_t} \sin(j\alpha + \tau) \\ \frac{\pi}{r_t} \cos(j\alpha + \tau) \\ \kappa \pm \frac{4\pi j}{a} \end{pmatrix}. \quad (26)$$

As in the case of the real nanotube, the transformations

$$\tilde{\mathcal{M}}_{s,j}^- = \tilde{\mathcal{T}}_s^- \tilde{\mathcal{T}}_j^+. \quad (27)$$

where  $s = 0, 1, \dots, n-1$ ,  $j = -L+s, \dots, L+s$ , generate a group,  $\tilde{\mathcal{G}}_{\tilde{A}}$ , and  $\tilde{\mathcal{M}}_{s,-L+s}^- \tilde{\mathcal{U}}_{\tilde{A}}^{00} = \tilde{\mathcal{M}}_{s,L+s}^- \tilde{\mathcal{U}}_{\tilde{A}}^{00}$ . A fundamental domain is the interior of the curved rhombus  $B_1B_2B_3B_4$  lying on the reciprocal tube and complemented by the sides  $B_1B_2$  and  $B_1B_4$  with the points  $B_2$  and  $B_4$  being excluded. The transformations  $\tilde{\mathcal{T}}_s^- \tilde{\mathcal{T}}_j^+$  map the unit cell  $\tilde{\mathcal{U}}_{\tilde{A}}^{00} = \tilde{\mathcal{U}}_{\tilde{A}}$  of the tube to all other rhombuses and

$$\bigcup_{s=0}^{n-1} \bigcup_{j=-L+s}^{L+s-1} \tilde{\mathcal{U}}_{\tilde{A}}^{sj} = \tilde{A}. \quad (28)$$

We next proceed with constructing the Brillouin zone of the reciprocal tube  $\tilde{A}$  by selecting the four rhombuses of the reciprocal tube which share the vortex  $B_1$ , the point  $(\tilde{r} = \tilde{r}_t, \theta = 0, \tilde{z} = 0)$  in the reciprocal space. On unrolling the reciprocal tube and drawing perpendicular bisectors of the lines joining the point  $B_1$  with the six closest vertices of the four rhombuses,  $B_2, B_3, B_4, B_5, B_6$ , and  $B_7$ , we get a nonregular hexagon (the deep blue hexagon in Fig. 2). Its area coincides with that of the rhombus  $B_1B_2B_3B_4$ . When rolled around the  $\tilde{z}$ -axis and placed on the reciprocal tube  $\tilde{A}$ , the polygon becomes an

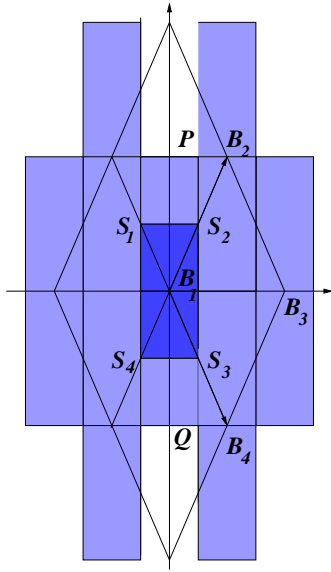


FIG. 3. Domain (the deep blue rectangle) of the transformations  $\tilde{\mathcal{T}}_j^\pm \mathbf{k}$  associated with an armchair nanotube  $\mathcal{A}$ .

analogue of the Brillouin zone for the tube reciprocal to an armchair nanotube.

To determine the domains of the transformations  $\tilde{\mathcal{T}}_j^+ \mathbf{k}$  and  $\tilde{\mathcal{T}}_j^- \mathbf{k}$ , we draw a rectangle by joining the midpoints of the four sides of the Brillouin hexagon which are also the midpoints of the segments  $B_1B_2$ ,  $B_1B_4$ ,  $B_1B_5$ , and  $B_1B_7$ . These points are the vertices of the rectangle  $\mathcal{K} = S_1S_2S_3S_4$  in Fig. 3, the domain of the transformations  $\tilde{\mathcal{T}}_j^+ \mathbf{k}$  and  $\tilde{\mathcal{T}}_j^- \mathbf{k}$ ,

$$\mathcal{K} = \left\{ \mathbf{k} \in \tilde{\mathcal{A}} : -\frac{2\pi}{a} \leq \kappa < \frac{2\pi}{a}, -\frac{\alpha}{2} \leq \tau < \frac{\alpha}{2} \right\}. \quad (29)$$

Because of the symmetry, this domain is shared by both transformations.

### III. STRUCTURE OF A CHIRAL NANOTUBE AND ITS RECIPROCAL

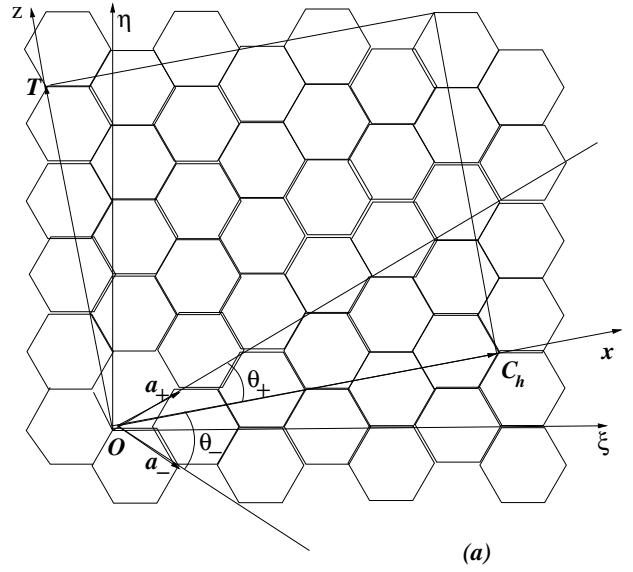
Consider a graphene sheet lying on the plane  $\Pi = \{|x| < \infty, y = r_t, |z| < \infty\}$  (Fig. 4a) when the chiral vector  $\mathbf{C}_h$  is

$$\mathbf{C}_h = (n, m) = n\mathbf{a}_+ + m\mathbf{a}_-, \quad (30)$$

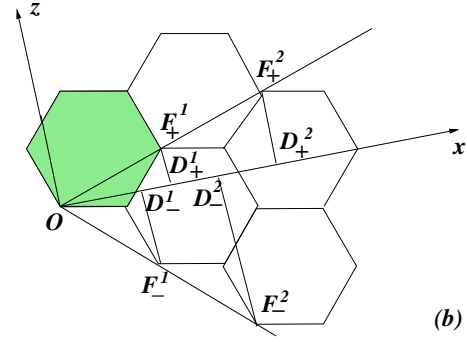
where  $n$  and  $m$  are integers,  $0 < m < n$ , and  $\mathbf{a}_\pm$  are the vectors (4) in the frame  $\xi O\eta$ . Notice that in this case the  $\xi$ - and  $\eta$ -axes do not coincide with the  $x$ - and  $z$ -axes as in Section II.

The angle between the vectors  $\mathbf{C}_h$  and  $\mathbf{a}_+$ , the chiral angle  $\theta_+$ , is given by [2]

$$\theta_+ = \cos^{-1} \frac{2n+m}{2\sqrt{n^2+m^2+nm}}. \quad (31)$$



(a)



(b)

FIG. 4. (a): Graphene sheet and the chiral and translation vectors  $\mathbf{C}_h$  and  $\mathbf{T}$ . (b): Projections of the vectors  $ja_\pm$  ( $j = 1, 2$ ) on the  $x$  and  $z$ -axes.

Simple calculations express the angle  $\theta_- = \frac{\pi}{3} - \theta_+$  between the vectors  $\mathbf{C}_h$  and  $\mathbf{a}_-$  through the chiral numbers  $n$  and  $m$  as

$$\theta_- = \cos^{-1} \frac{n+2m}{2\sqrt{n^2+m^2+nm}}. \quad (32)$$

The chiral vector  $\mathbf{C}_h$  is complemented by the translation vector  $\mathbf{T}$  [2] orthogonal to  $\mathbf{C}_h$ , directing along the  $z$ -axis and defined by

$$\mathbf{T} = (t_1, t_2) = t_1\mathbf{a}_+ + t_2\mathbf{a}_-, \quad (33)$$

where

$$t_1 = \frac{n+2m}{d_R}, \quad t_2 = -\frac{2n+m}{d_R}. \quad (34)$$

The number  $d_R$  is expressed through the greatest common divisor  $d$  of the integers  $n+2m$  and  $2n+m$  as follows. If  $n-m$  is a multiple of  $3d$ , then  $d_R = 3d$ . Otherwise,  $d_R = d$ .

By rolling up the graphene sheet defined by the two vectors  $\mathbf{C}_h$  and  $\mathbf{T}$  and lying in the plane  $\Pi = \{y = r_t\}$

around the  $z$ -axis passing through the point  $x = z = 0$  we construct a chiral nanotube  $\mathcal{A} = \mathcal{A}(n, m)$ . The circumference and radius  $r_t$  of a cross-section of the tube orthogonal to its axis are

$$|\mathbf{C}_h| = a\sqrt{n^2 + m^2 + nm}, \quad r_t = \frac{|\mathbf{C}_h|}{2\pi}, \quad (35)$$

while the nanotube length is

$$|\mathbf{T}| = \frac{\sqrt{3}a}{d_R} \sqrt{n^2 + m^2 + nm}. \quad (36)$$

The nanotube designed can be extended along the  $z$ -axis to have the length  $q|\mathbf{T}|$ ,  $q$  is a positive real number. The number of cells in the whole nanotube,  $N$ , is assumed to be a multiple of  $2m$ ,  $N = 2mL$ .

Referring to the unrolled nanotube formed by the vectors  $\mathbf{C}_h$  and  $\mathbf{T}$  we define the projections  $OD_{\pm}^j$  and  $F_{\pm}^j D_{\pm}^j$  of the vectors  $j\mathbf{a}_{\pm}$  on the  $x$ - and  $z$ -axes, respectively (Fig. 4b). They are

$$OD_{\pm}^j = ja \cos \theta_{\pm},$$

$$F_{\pm}^j D_{\pm}^j = \pm ja \sin \theta_{\pm}, \quad j = 1, 2, \dots \quad (37)$$

When the sheet is rolled up and the nanotube is formed, the projections  $OD_{\pm}^1$  and  $OD_{\mp}^1$  on the  $x$ -axis become circular arcs and

$$r_t \alpha_{\pm} = a \cos \theta_{\pm}, \quad (38)$$

where  $\alpha_{\pm}$  are the angles of rotation of the points  $D_{\pm}^1$  around the tube axis when the point  $O = (0, r_t, 0)$  is fixed. This and formulas (31) and (32) yield the angles of rotation

$$\begin{aligned} \alpha_+ &= \frac{\pi(2n + m)}{n^2 + m^2 + nm}, \\ \alpha_- &= \frac{\pi(n + 2m)}{n^2 + m^2 + nm}. \end{aligned} \quad (39)$$

The lattice vectors  $\mathbf{a}_+$  and  $\mathbf{a}_-$  become elliptical arcs, and their chords have the lengths (Table II)

$$a_{\pm}^{\circ} = \sqrt{a^2 \sin^2 \theta_{\pm} + 4r_t^2 \sin^2 \frac{\alpha_{\pm}}{2}}. \quad (40)$$

Introduce next the characteristic vectors of the chiral nanotube  $\mathcal{A}$ , analogues of the armchair vectors (8),

$$\hat{\mathbf{a}}_+ = \begin{pmatrix} -r_t \sin \alpha_+ \\ r_t \cos \alpha_+ \\ c_+ \end{pmatrix}, \quad \hat{\mathbf{a}}_- = \begin{pmatrix} -r_t \sin \alpha_- \\ r_t \cos \alpha_- \\ -c_- \end{pmatrix} \quad (41)$$

TABLE II. The parameters  $a_{\pm}^* = a_{\pm}^{\circ}/a$  for some chiral nanotubes.

$\mathbf{C}_h$	(4,2)	(6,1)	(6,5)	(7,4)	(8,3)
$a_+^*$	0.9540	0.9635	0.9887	0.9867	0.9854
$a_-^*$	0.9811	0.9947	0.9911	0.9936	0.9957

where  $\pm c_{\pm}$  are the projections of the vectors  $\mathbf{a}_{\pm}$  on the nanotube axis and

$$c_+ = a \sin \theta_+ = \frac{\sqrt{3}ma}{2\sqrt{n^2 + m^2 + nm}},$$

$$c_- = a \sin \theta_- = \frac{\sqrt{3}na}{2\sqrt{n^2 + m^2 + nm}}. \quad (42)$$

We also need analogues of the reciprocal armchair vectors (9) in the reciprocal space  $\tilde{R}^3$ . They are

$$\tilde{\mathbf{b}}_+ = \begin{pmatrix} -\frac{\pi}{r_t} \sin \alpha_+ \\ \frac{\pi}{r_t} \cos \alpha_+ \\ \frac{2\pi}{c_+} \end{pmatrix}, \quad \tilde{\mathbf{b}}_- = \begin{pmatrix} -\frac{\pi}{r_t} \sin \alpha_- \\ \frac{\pi}{r_t} \cos \alpha_- \\ -\frac{2\pi}{c_-} \end{pmatrix}. \quad (43)$$

The real and reciprocal vectors  $\hat{\mathbf{a}}_{\pm}$  and  $\tilde{\mathbf{b}}_{\mp}$  are not mutually orthogonal and

$$\hat{\mathbf{a}}_{\pm} \cdot \tilde{\mathbf{b}}_{\pm} = 3\pi,$$

$$\hat{\mathbf{a}}_{\pm} \cdot \tilde{\mathbf{b}}_{\mp} = \pi \cos(\alpha_+ - \alpha_-) - 2\pi \frac{c_{\pm}}{c_{\mp}}. \quad (44)$$

We select the hexagon of the unrolled nanotube  $\mathcal{A}$  with the vertices  $O$  and  $F_+^1$  (it is shadowed in Fig. 4b) as the preimage of the unit cell of the tube. The unit cell of the nanotube,  $\mathcal{U}_{\mathcal{A}}$ , is this hexagon rolled around the  $z$ -axis passing through the point  $O_t$ . If the integers  $n$  and  $m$  satisfy the condition  $0 < m < n$ , then all the sides of the unit cell  $\mathcal{U}_{\mathcal{A}}$  are elliptical arcs.

Introduce now the rotation-translation transformations

$$\mathcal{T}_j^{\pm} \mathbf{r} = \begin{pmatrix} -r_t \sin(j\alpha_{\pm} + \theta) \\ r_t \cos(j\alpha_{\pm} + \theta) \\ z \pm jc_{\pm} \end{pmatrix}, \quad j = \pm 1, \pm 2, \dots, \quad (45)$$

with  $\mathcal{T}_0^{\pm}$  being the identity map and  $\mathbf{r}$  being the vector (11) confined to the unit cell  $\mathcal{U}_{\mathcal{A}}$ . It becomes evident that if  $s = 0, 1, \dots, m-1$  and  $j = -L+s, -L+s+1, \dots, L+s-1$ , then the transformations  $\mathcal{M}_{s,j}^{-+}$  map the unit cell to all hexagons of the nanotube  $\mathcal{A}(n, m)$ , and each hexagon in  $\mathcal{A}$  is uniquely assigned to a pair  $(s, j)$  provided  $\mathcal{M}_{s,-L+s}^{-+} \mathcal{U}_{\mathcal{A}}^{00} = \mathcal{M}_{s,L+s}^{-+} \mathcal{U}_{\mathcal{A}}^{00}$ . Here,  $\mathcal{M}_{s,j}^{-+}$  are the transformations (16) associated with the chiral nanotube  $\mathcal{A}(n, m)$ .

As before, the transformations  $\mathcal{M}_{s,j}^{-+}$  ( $s = 0, 1, \dots, m-1$ ,  $j = -L+s, -L+s+1, \dots, L+s-1$ ) generate a space group  $\mathcal{G}_{\mathcal{A}}$ . We remark that another one-to-one correspondence between the pair  $(j, s)$  and the cell  $U_{\mathcal{A}}^{js}$  is obtained if the transformations  $\mathcal{M}_{j,s}^{+-} = \mathcal{T}_j^+ \mathcal{T}_s^-$  are applied. Here,  $j = 0, 1, \dots, n-1$  and  $s = -L'+j, -L'+j+1, \dots, L'+j-1$ . In this case we assume that the number of cells  $N$  is a multiple of  $2n$ ,  $N = 2nL'$ .

Consider next the reciprocal tube  $\tilde{\mathcal{A}}$  associated with the reciprocal vectors (43). Its radius is  $\tilde{r}_t = \pi/r_t$ . To

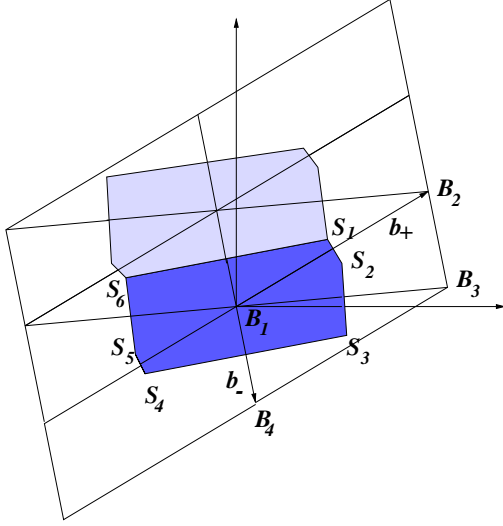


FIG. 5. Chiral symmetry: the unrolled parallelogram of periods  $B_1B_2B_3B_4$  of the reciprocal tube  $\tilde{\mathcal{A}}$ , and the Brillouin hexagon  $S_1S_2\dots S_6$ .

describe its unit cell, as in the armchair nanotube case, consider a reciprocal lattice on the reciprocal plane  $\tilde{R}^2$  characterized by the lattice vectors  $\mathbf{b}_\pm = \langle b'_\pm, b''_\pm \rangle$ . The second components of the vectors are

$$b''_+ = \frac{2\pi}{c_+}, \quad b''_- = -\frac{2\pi}{c_-}. \quad (46)$$

Since  $0 < \theta_+ < \theta_- < \frac{\pi}{3}$ , we have  $0 < c_+ < c_-$  and therefore  $b''_+ > |b''_-|$ . The first components of the vectors  $\mathbf{b}_\pm$  are fixed by the condition

$$\alpha_\pm \tilde{r}_t = b'_\pm \quad (47)$$

and formulas (35) and (39). We find

$$b'_+ = \frac{2\pi^3(2n+m)}{a(n^2+m^2+nm)^{3/2}},$$

$$b'_- = \frac{2\pi^3(n+2m)}{a(n^2+m^2+nm)^{3/2}} < b'_+. \quad (48)$$

One of the possible choices for a unit cell of the reciprocal tube  $\tilde{\mathcal{A}}$ ,  $\tilde{\mathcal{U}}_{\tilde{\mathcal{A}}} = \tilde{\mathcal{U}}_{\tilde{\mathcal{A}}}^{00}$ , is the image of the parallelogram  $B_1B_2B_3B_4$  formed by the vectors  $\mathbf{b}_+ = B_1B_2$  and  $\mathbf{b}_- = B_1B_4$  and rolled around the reciprocal tube  $\tilde{\mathcal{A}}$  (Fig. 5). By means of compositions of the transformations  $\tilde{\mathcal{T}}_j^+$  and  $\tilde{\mathcal{T}}_s^-$ ,  $\mathcal{M}_{s,j}^{-+} = \tilde{\mathcal{T}}_s^- \tilde{\mathcal{T}}_j^+$ , defined in the reciprocal space  $\tilde{R}^3$  as

$$\tilde{\mathcal{T}}_j^\pm \mathbf{k} = \begin{pmatrix} -\frac{\pi}{r_t} \sin(j\alpha_\pm + \tau) \\ \frac{\pi}{r_t} \cos(j\alpha_\pm + \tau) \\ \kappa \pm \frac{2\pi j}{c_\pm} \end{pmatrix} \quad (49)$$

we may establish a one-to-one correspondence between the pair  $(s, j)$  ( $s = 0, 1, \dots, m-1$ ,  $j = -L+s, \dots, L+s-1$ ) and all the unit cells  $\tilde{\mathcal{U}}_{\tilde{\mathcal{A}}}^{js}$  of the reciprocal tube.

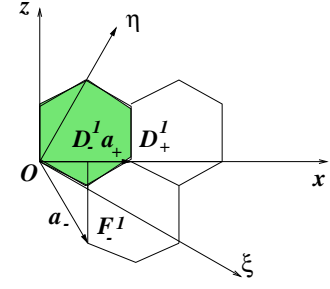


FIG. 6. An unrolled zigzag nanotube

As for the armchair reciprocal tube, we construct the first Brillouin zone, a hexagonal unit cell centered at the vertex  $B_1$  shared by the four neighboring parallelogram-like cells of the reciprocal tube  $\tilde{\mathcal{A}}$  (Fig. 5). When unrolled, the four cells become parallelograms. The bisectors orthogonal to the lines joining the origin  $B_1$  of the reciprocal coordinates  $\tilde{x}, \tilde{z}$  with the six nearest lattice points form a polygon. It is the hexagon  $S_1S_2\dots S_6$  (Fig. 5), and its area and the area of the parallelogram  $B_1B_2B_3B_4$  are the same. The hexagonal cell is symmetric with respect to the origin  $B_1$ . When the hexagon is mapped back to the reciprocal tube  $\tilde{\mathcal{A}}$  by rolling it around its axis, the  $\tilde{z}$ -axis passing through the origin of the reciprocal space, another reciprocal unit cell is formed. It is the first Brillouin zone.

In the chiral case, the domains of the transformations  $\tilde{\mathcal{T}}_j^+ \mathbf{k}$  and  $\tilde{\mathcal{T}}_j^- \mathbf{k}$ ,  $\mathcal{K}^+$  and  $\mathcal{K}^-$ , do not coincide. They are determined from the unrolled Brillouin zone by dropping perpendiculars from the midpoints of the sides  $S_1S_2$  and  $S_4S_5$  for  $\mathcal{K}^+$  and  $S_1S_6$  and  $S_3S_4$  for  $\mathcal{K}^-$  on the reciprocal lattice axes. These domains are

$$\mathcal{K}^\pm = \left\{ \mathbf{k} \in \tilde{\mathcal{A}} : -\frac{\pi}{c_\pm} \leq \kappa < \frac{\pi}{c_\pm}, -\frac{\alpha_\pm}{2} \leq \tau < \frac{\alpha_\pm}{2} \right\}. \quad (50)$$

#### IV. ZIGZAG NANOTUBE AND ITS RECIPROCAL

A zigzag nanotube,  $\mathcal{A}$ , is characterized by the chiral vector  $\mathbf{C}_h = (n, 0)$ . The graphene sheet associated with the unrolled tube is placed on the plane  $xOz$ ,  $y = r_t$ , and the frame  $\xi O\eta$  forms an angle  $\frac{\pi}{6}$  with the frame  $xOz$  (Fig. 6). From the general formulas for a chiral nanotube  $\mathbf{C}_h(n, m)$  we immediately compute the radius  $r_t$ , the angles  $\theta_\pm$ , and the projections of the vectors  $\mathbf{a}_\pm$  on the axis  $Ox$  and  $Oz$ . They are

$$r_t = \frac{na}{2\pi}, \quad \theta_+ = 0, \quad \theta_- = \frac{\pi}{3},$$

$$F_+^1 D_+^1 = 0, \quad F_-^1 D_-^1 = -\frac{\sqrt{3}a}{2},$$

$$OD_+^1 = a, \quad OD_-^1 = \frac{a}{2}. \quad (51)$$

When the point  $O$  is fixed and the graphene sheet is rolled up to form a zigzag nanotube, the points  $D_{\pm}^1$  rotate around the tube axis, and the angles of rotations  $\alpha_{\pm}$  have the values

$$\alpha_+ = \frac{2\pi}{n}, \quad \alpha_- = \frac{\pi}{n}. \quad (52)$$

As a result, the lattice vectors  $\mathbf{a}_+$  and  $\mathbf{a}_-$  become a circular and elliptic arc whose chords are of lengths  $a_+^{\circ}$  and  $a_-^{\circ}$ , respectively,

$$a_+^{\circ} = \frac{an}{\pi} \sin \frac{\pi}{n},$$

$$a_-^{\circ} = a \sqrt{\frac{3}{4} + \frac{n^2}{\pi^2} \sin^2 \frac{\pi}{2n}}. \quad (53)$$

Their values for sample zigzag nanotubes are given in Table III.

For a zigzag nanotube, the parameters  $c_{\pm}$  given by (42) have the values  $c_+ = 0$  and  $c_- = \frac{\sqrt{3}a}{2}$ , and the characteristic vectors  $\hat{\mathbf{a}}_{\pm}$  of the real zigzag nanotube  $\mathcal{A}$  and the vectors  $\tilde{\mathbf{b}}_{\pm}$  of the reciprocal tube  $\tilde{\mathcal{A}}$  become

$$\hat{\mathbf{a}}_+ = \begin{pmatrix} -r_t \sin \frac{2\pi}{n} \\ r_t \cos \frac{2\pi}{n} \\ 0 \end{pmatrix}, \quad \hat{\mathbf{a}}_- = \begin{pmatrix} -r_t \sin \frac{\pi}{n} \\ r_t \cos \frac{\pi}{n} \\ -\frac{\sqrt{3}a}{2} \end{pmatrix} \quad (54)$$

and

$$\tilde{\mathbf{b}}_+ = \begin{pmatrix} -\frac{\pi}{r_t} \sin \frac{2\pi}{n} \\ \frac{\pi}{r_t} \cos \frac{2\pi}{n} \\ 0 \end{pmatrix}, \quad \tilde{\mathbf{b}}_- = \begin{pmatrix} -\frac{\pi}{r_t} \sin \frac{\pi}{n} \\ \frac{\pi}{r_t} \cos \frac{\pi}{n} \\ -\frac{4\pi}{\sqrt{3}a} \end{pmatrix}. \quad (55)$$

In the case of a zigzag nanotube, the transformation  $\mathcal{T}_j^+$  is a pure rotation,

$$\mathcal{T}_j^+ \mathbf{r} = \begin{pmatrix} -r_t \sin(\frac{2\pi j}{n} + \theta) \\ r_t \cos(\frac{2\pi j}{n} + \theta) \\ z \end{pmatrix}, \quad (56)$$

while the second transformation  $\mathcal{T}_j^-$  is a rotation-translation,

$$\mathcal{T}_j^- \mathbf{r} = \begin{pmatrix} -r_t \sin(\frac{\pi j}{n} + \theta) \\ r_t \cos(\frac{\pi j}{n} + \theta) \\ z - \frac{\sqrt{3}aj}{2} \end{pmatrix}, \quad j = \pm 1, \pm 2, \dots \quad (57)$$

The shadowed hexagon (Fig. 6) rolled around the nanotube is chosen as a unit cell  $\mathcal{U}_{\mathcal{A}} = \mathcal{U}_{\mathcal{A}}^{00}$ . For zigzag nanotubes, the number of cells in the tube is a multiple of  $2n$ ,

TABLE III. The parameters  $a_{\pm}^* = a_{\pm}^{\circ}/a$  for some zigzag nanotubes.

$\mathbf{C}_h$	(5,0)	(6,0)	(8,0)	(10,0)	(20,0)
$a_+^*$	0.9355	0.9549	0.9745	0.9836	0.9959
$a_-^*$	0.9959	0.9972	0.9984	0.9990	0.9997

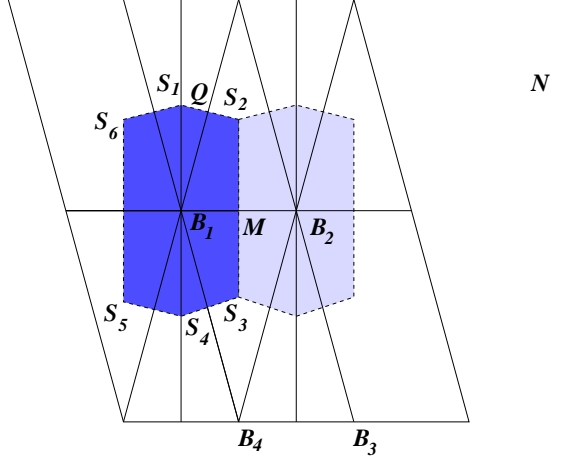


FIG. 7. Zigzag symmetry: the parallelogram of periods  $B_1 B_2 B_3 B_4$  of the unrolled reciprocal tube  $\tilde{\mathcal{A}}$ , and the Brillouin hexagon  $S_1 S_2 \dots S_6$ .

$N = 2nL$ . The transformations  $\mathcal{M}_{j,s}^{+-}$  ( $j = 0, 1, \dots, n-1$ ,  $s = -L, -L+1, \dots, L-1$ ) generate a space group  $\mathcal{G}_{\mathcal{A}}$  and map the unit cell  $\mathcal{U}_{\mathcal{A}}$  to all cells  $\mathcal{U}_{\mathcal{A}}^{js}$ . It is evident that there is a one-to-one correspondence between the pair  $(j, s)$  and the cell  $\mathcal{U}_{\mathcal{A}}^{js}$  provided  $j = 0, 1, \dots, n-1$ ,  $s = -L, -L+1, \dots, L-1$ , and  $\mathcal{M}_{j,-L}^{+-} \mathcal{U}_{\mathcal{A}}^{00} = \mathcal{M}_{j,L}^{+-} \mathcal{U}_{\mathcal{A}}^{00}$ .

The reciprocal tube  $\tilde{\mathcal{A}}$  of the zigzag nanotube  $\mathcal{A}$  has radius  $\tilde{r}_t = \frac{2\pi^2}{na}$  and the associated transformations are

$$\tilde{\mathcal{T}}_j^+ \mathbf{k} = \begin{pmatrix} -\tilde{r}_t \sin(\frac{2\pi j}{n} + \tau) \\ \tilde{r}_t \cos(\frac{2\pi j}{n} + \tau) \\ \kappa \end{pmatrix} \quad (58)$$

and

$$\tilde{\mathcal{T}}_j^- \mathbf{k} = \begin{pmatrix} -\tilde{r}_t \sin(\frac{\pi j}{n} + \tau) \\ \tilde{r}_t \cos(\frac{\pi j}{n} + \tau) \\ \kappa - \frac{4\pi j}{\sqrt{3}a} \end{pmatrix}, \quad j = \pm 1, \pm 2, \dots \quad (59)$$

The parallelogram of periods  $B_1 B_2 B_3 B_4$  of the unrolled reciprocal tube  $\tilde{\mathcal{A}}$  is defined by the vectors  $\mathbf{b}_{\pm} = \langle b'_{\pm}, b''_{\pm} \rangle$  of the reciprocal lattice in the plane  $\tilde{R}^2$  (Fig. 7). Formulas (55) immediately yield

$$nb'_+ = 2nb'_- = 2\pi\tilde{r}_t,$$

$$b''_+ = 0, \quad b''_- = -\frac{4\pi}{\sqrt{3}a}, \quad (60)$$

and therefore

$$\mathbf{b}_+ = \langle \frac{4\pi^3}{n^2 a}, 0 \rangle, \quad \mathbf{b}_- = \langle \frac{2\pi^3}{n^2 a}, -\frac{4\pi}{\sqrt{3}a} \rangle. \quad (61)$$

If we consider the four parallelograms which share the vertex  $B_1$  and draw the bisectors orthogonal to the lines joining the origin  $B_1$  to the nearest six lattice points,

we form a hexagon  $S_1S_2\dots S_6$  (Fig. 7). It has the same area as the parallelogram  $B_1B_2B_3B_4$  and can also be chosen as a unit cell of the lattice (the deep blue hexagon in Fig. 7). When rolled around the axis of the reciprocal tube to be a part of it, the transformed hexagon becomes a unit cell  $\mathcal{U}_{\tilde{\mathcal{A}}}$  of the reciprocal tube  $\tilde{\mathcal{A}}$ . This is the Brillouin zone of the tube reciprocal to the zigzag nanotube  $\mathcal{A}(n, 0)$ . On joining the midpoints of the sides  $S_1S_2$ ,  $S_3S_4$ ,  $S_4S_5$ , and  $S_1S_6$ , we draw a rectangle whose height and width are  $2|b''_-|$  and  $2b'_-$ , respectively. From this rectangle we determine the domain of the transformation  $\mathcal{T}^- \mathbf{k}$

$$\mathcal{K}^- = \left\{ \mathbf{k} \in \tilde{\mathcal{A}} : -\frac{2\pi}{\sqrt{3}a} \leq \kappa < \frac{2\pi}{\sqrt{3}a}, -\frac{\pi}{2n} \leq \tau < \frac{\pi}{2n} \right\}. \quad (62)$$

The domain of the transformation  $\mathcal{T}^+ \mathbf{k}$ , a rotation transformation in the reciprocal space, is defined by

$$\mathcal{K}^+ = \left\{ \mathbf{k} \in \tilde{\mathcal{A}} : \kappa = \text{const}, -\frac{\pi}{n} \leq \tau < \frac{\pi}{n} \right\}. \quad (63)$$

## V. ANALOGUE OF THE BLOCH THEORY FOR A SWCNT

### A. Analogue of the Bloch theorem

**Theorem 1.** Let  $\mathcal{A} = \mathcal{A}(n, m)$  be a SWCNT characterized by the chiral vector  $\mathbf{C}_h(n, m)$ . Suppose the potential  $\mathcal{V}(\mathbf{r})$  of the Hamiltonian

$$\mathcal{H} = -\frac{\hbar^2}{2m} \nabla^2 + \mathcal{V}(\mathbf{r}) \quad (64)$$

of a single electron has the rotation-translation symmetry of the nanotube

$$\mathcal{V}(\mathcal{T}_j^\pm \mathbf{r}) = \mathcal{V}(\mathbf{r}), \quad j = \pm 1, \pm 2, \dots, \quad (65)$$

where the transformations  $\mathcal{T}_j^\pm$  are defined on the nanotube  $\mathcal{A}(n, m)$  by (45),  $\mathbf{r} \in \mathcal{U}_{\mathcal{A}}$  is the vector (11), and  $\mathcal{U}_{\mathcal{A}}$  is a unit curved hexagonal cell of the nanotube. Then any solution of the Schrödinger equation

$$\mathcal{H}\psi(\mathbf{r}; \mathbf{k}) = \epsilon(\mathbf{k})\psi(\mathbf{r}; \mathbf{k}) \quad (66)$$

satisfies the relations

$$\psi(\mathcal{T}_j^\pm \mathbf{r}; \tilde{\mathcal{T}}_j^\pm \mathbf{k}) = \exp \left\{ \pm ij \left( \kappa c_\pm + \frac{2\pi z}{c_\pm} \right) \right\} \psi(\mathbf{r}; \mathbf{k}), \quad (67)$$

and, in particular,

$$\psi(\mathcal{T}_j^\pm \mathbf{r}; \mathbf{k}) = e^{\pm ij\kappa c_\pm} \psi(\mathbf{r}; \mathbf{k}), \quad j = \pm 1, \pm 2, \dots \quad (68)$$

Here,  $c_\pm$  are the real parameters (42),  $\mathbf{k} \in \tilde{\mathcal{K}}^\pm$  is the vector (24),  $\mathcal{K}^\pm$  are the domains (50), and  $\tilde{\mathcal{T}}_j^\pm$  are the transformations (49) defined on the reciprocal tube.

Moreover, if the function  $\psi(\mathbf{r}; \mathbf{k})$  is written as

$$\psi(\mathbf{r}; \mathbf{k}) = e^{i\mathbf{k} \cdot \mathbf{r}} u(\mathbf{r}; \mathbf{k}), \quad (69)$$

then the function  $u(\mathbf{r}; \mathbf{k})$  is invariant with respect to the composition of the transformations  $\mathcal{T}_j^\pm$  and  $\tilde{\mathcal{T}}_j^\pm$ ,

$$u(\mathcal{T}_j^\pm \mathbf{r}; \tilde{\mathcal{T}}_j^\pm \mathbf{k}) = u(\mathbf{r}; \mathbf{k}), \quad j = \pm 1, \pm 2, \dots \quad (70)$$

In particular, if the nanotube has the armchair symmetry,  $\mathcal{A} = \mathcal{A}(n, n)$ , then the relations (67) have the form

$$\psi(\mathcal{T}_j^\pm \mathbf{r}; \tilde{\mathcal{T}}_j^\pm \mathbf{k}) = \exp \left\{ \pm ij \left( \frac{\kappa a}{2} + \frac{4\pi z}{a} \right) \right\} \psi(\mathbf{r}; \mathbf{k}),$$

$$\mathbf{k} \in \mathcal{K}, \quad j = \pm 1, \pm 2, \dots, \quad (71)$$

the transformations  $\mathcal{T}_j^\pm$  and  $\tilde{\mathcal{T}}_j^\pm$  are given by (15) and (26), while  $\mathcal{K}$  is the domain (29).

For a zigzag nanotube  $\mathcal{A} = \mathcal{A}(n, 0)$ , the relations (67) read

$$\psi(\mathcal{T}_j^+ \mathbf{r}; \tilde{\mathcal{T}}_j^+ \mathbf{k}) = \psi(\mathbf{r}; \mathbf{k}), \quad \mathbf{k} \in \mathcal{K}^+,$$

$$\psi(\mathcal{T}_j^- \mathbf{r}; \tilde{\mathcal{T}}_j^- \mathbf{k}) = \exp \left\{ -ij \left( \frac{\sqrt{3}\kappa a}{2} + \frac{4\pi z}{\sqrt{3}a} \right) \right\} \psi(\mathbf{r}; \mathbf{k}),$$

$$\mathbf{k} \in \mathcal{K}^-, \quad j = \pm 1, \pm 2, \dots \quad (72)$$

where  $\mathcal{T}_j^+ = \tilde{\mathcal{T}}_j^+ = \mathcal{R}_j$  are the rotation transformations

$$\mathcal{R}_j = \begin{pmatrix} \cos j\alpha & -\sin j\alpha & 0 \\ \sin j\alpha & \cos j\alpha & 0 \\ 0 & 0 & 1 \end{pmatrix}, \quad (73)$$

$\mathcal{T}_j^-$  and  $\tilde{\mathcal{T}}_j^-$  are the rotation-translation transformations in the real and reciprocal spaces given by (57) and (59), and  $\mathcal{K}^-$  and  $\mathcal{K}^+$  are the domains defined in (62) and (63), respectively.

*Proof.* Let  $f(\mathbf{r}; \mathbf{k})$  be a function of  $\mathbf{r}$  and  $\mathbf{k}$ , the radius-vectors of points on the real and reciprocal tubes  $\mathcal{A}$  and  $\tilde{\mathcal{A}}$ , respectively. Define the rotation-translation transformations of the function  $f(\mathbf{r}; \mathbf{k})$  by

$$\mathcal{T}_j^\pm f(\mathbf{r}; \mathbf{k}) = f(\mathcal{T}_j^\pm \mathbf{r}; \mathbf{k}),$$

$$\tilde{\mathcal{T}}_j^\pm f(\mathbf{r}; \mathbf{k}) = f(\mathbf{r}; \tilde{\mathcal{T}}_j^\pm \mathbf{k}). \quad (74)$$

Denote by  $\psi(\mathbf{r}; \mathbf{k})$  an eigenfunction of the transformations  $\mathcal{T}_j^\pm$  in the real space,

$$\mathcal{T}_j^\pm \psi(\mathbf{r}; \mathbf{k}) = \lambda_j^\pm(\mathbf{k}) \psi(\mathbf{r}; \mathbf{k}). \quad (75)$$

Simultaneously, it is an eigenfunction of transformation  $\tilde{\mathcal{T}}_j^\pm$  in the reciprocal space,

$$\tilde{\mathcal{T}}_j^\pm \psi(\mathbf{r}; \mathbf{k}) = \mu_j^\pm(\mathbf{r}) \psi(\mathbf{r}; \mathbf{k}), \quad (76)$$

that is

$$\mathcal{T}_j^\pm \tilde{\mathcal{T}}_j^\pm \psi(\mathbf{r}; \mathbf{k}) = \lambda_j^\pm(\mathbf{k}) \mu_j^\pm(\mathbf{r}) \psi(\mathbf{r}; \mathbf{k}). \quad (77)$$

As in the Bloch theory for flat lattices, the electron distribution  $|\psi(\mathbf{r}; \mathbf{k})|$  has to have the same rotation-translation periodic properties as the potential (65). Therefore

$$|\mathcal{T}_j^\pm \tilde{\mathcal{T}}_j^\pm \psi(\mathbf{r}; \mathbf{k})| = |\psi(\mathbf{r}; \mathbf{k})|. \quad (78)$$

This implies that the eigenvalues  $\lambda_j^\pm(\mathbf{k})$  and  $\mu_j^\pm(\mathbf{r})$  have the form

$$\lambda_j^\pm(\mathbf{k}) = e^{i\sigma_j^\pm(\mathbf{k})}, \quad \mu_j^\pm(\mathbf{r}) = e^{i\eta_j^\pm(\mathbf{r})}, \quad (79)$$

where the arguments  $\sigma_j^\pm(\mathbf{k})$  and  $\eta_j^\pm(\mathbf{r})$  are invariant to the rotations  $\mathcal{R}_j$ . Since the translations in the transformations  $\mathcal{T}_j^\pm$  and  $\tilde{\mathcal{T}}_j^\pm$  are applied along the  $z$  and  $\tilde{z}$ -axes of the real and reciprocal spaces  $R^3$  and  $\tilde{R}^3$ , respectively, and because of formulas (45) and (49) and the following relations for compositions of the transformations  $\mathcal{T}_j^\pm$  and  $\tilde{\mathcal{T}}_j^\pm$ :

$$\begin{aligned} \mathcal{T}_j^\pm \tilde{\mathcal{T}}_j^\pm \mathcal{T}_l^\pm \tilde{\mathcal{T}}_l^\pm \psi(\mathbf{r}; \mathbf{k}) &= \psi(\mathcal{T}_{j+l}^\pm \mathbf{r}; \tilde{\mathcal{T}}_{j+l} \mathbf{k}) \\ &= \lambda_j(\mathbf{k}) \lambda_l(\mathbf{k}) \mu_j(\mathbf{r}) \mu_l(\mathbf{r}) \psi(\mathbf{r}; \mathbf{k}) \\ &= \lambda_{j+l}(\mathbf{k}) \mu_{j+l}(\mathbf{r}) \psi(\mathbf{r}; \mathbf{k}), \end{aligned} \quad (80)$$

we deduce

$$\sigma_j^\pm(\mathbf{k}) = \pm \kappa c_\pm j, \quad \eta_j^\pm(\mathbf{r}) = \pm \frac{2\pi z j}{c_\pm}. \quad (81)$$

It is evident that the Hamiltonian operator commutes with the transformations  $\mathcal{T}_j^\pm$  defined on the real tube  $\mathcal{A}$ . Also, it commutes with the transformations

$$e^{-i\eta_j^\pm(\mathbf{r})} \tilde{\mathcal{T}}_j^\pm = \exp\left(\mp \frac{2\pi iz j}{c_\pm}\right) \tilde{\mathcal{T}}_j^\pm, \quad (82)$$

that is

$$\left[ \exp\left(\mp \frac{2\pi iz j}{c_\pm}\right) \tilde{\mathcal{T}}_j^\pm \mathcal{T}_j^\pm, \mathcal{H} \right] = 0. \quad (83)$$

Therefore, without loss of generality, the eigenfunction chosen before may be considered as a solution of the wave equation (65). This implies that the relation

$$\mathcal{T}_j^\pm \tilde{\mathcal{T}}_j^\pm \psi(\mathbf{r}; \mathbf{k}) = \exp\left\{\pm ij \left(\kappa c_\pm + \frac{2\pi z}{c_\pm}\right)\right\} \psi(\mathbf{r}; \mathbf{k}) \quad (84)$$

holds, and formula (67) is proved. If the transformations  $\tilde{\mathcal{T}}_j \mathbf{k}$  are bypassed, then instead of formula (67) we have the relation (68).

Introduce next a function  $u(\mathbf{r}; \mathbf{k})$  such that  $\psi(\mathbf{r}; \mathbf{k}) = e^{i\mathbf{k} \cdot \mathbf{r}} u(\mathbf{r}; \mathbf{k})$  and compute the scalar product

$$\mathcal{T}_j^\pm \mathbf{r} \cdot \tilde{\mathcal{T}}_j^\pm \mathbf{k}$$

$$= \pi \cos(\theta - \tau) + \kappa z \pm c_\pm \kappa j \pm \frac{2\pi z j}{c_\pm} + 2\pi j^2. \quad (85)$$

Since

$$\mathbf{k} \cdot \mathbf{r} = \pi \cos(\theta - \tau) + \kappa z, \quad (86)$$

we deduce

$$e^{i\mathcal{T}_j^\pm \mathbf{r} \cdot \tilde{\mathcal{T}}_j^\pm \mathbf{k}} = \exp\left\{i \left(\mathbf{k} \cdot \mathbf{r} \pm c_\pm \kappa j \pm \frac{2\pi z j}{c_\pm}\right)\right\}. \quad (87)$$

By applying the transformations  $\mathcal{T}_j^\pm \tilde{\mathcal{T}}_j^\pm$  to the function  $\psi(\mathbf{r}; \mathbf{k})$  we obtain

$$\begin{aligned} \psi(\mathcal{T}_j^\pm \mathbf{r}; \tilde{\mathcal{T}}_j^\pm \mathbf{k}) &= e^{i\mathbf{k} \cdot \mathbf{r}} e^{\pm ij(c_\pm \kappa + 2\pi z/c_\pm)} u(\mathcal{T}_j^\pm \mathbf{r}; \tilde{\mathcal{T}}_j^\pm \mathbf{k}) \\ &= e^{\pm ij(c_\pm \kappa + 2\pi z/c_\pm)} \psi(\mathbf{r}; \mathbf{k}) \\ &= e^{\pm ij(c_\pm \kappa + 2\pi z/c_\pm)} e^{i\mathbf{k} \cdot \mathbf{r}} u(\mathbf{r}; \mathbf{k}), \end{aligned} \quad (88)$$

and the periodicity property (70) of the function  $u(\mathbf{r}; \mathbf{k})$  becomes evident.

Formulas (71) and (72) immediately follow from the general relations (67) if we put  $c_\pm = \frac{a}{2}$  for the armchair symmetry and  $c_+ = 0$  and  $c_- = \frac{\sqrt{3}a}{2}$  for the zigzag case. The theorem is proved.

*Remark.* If the transformations  $\tilde{\mathcal{T}}_j^\pm \mathbf{k}$  on the reciprocal tube are ignored, then the second part of Theorem 1 for SWCNTs, formula (69), is invalid. Indeed, since

$$e^{i\mathbf{k} \cdot \mathcal{T}_j^\pm \mathbf{r}} = e^{i[\pi \cos(j\alpha + \theta - \tau) + \kappa z]} e^{\pm ij\kappa c_\pm}, \quad (89)$$

there is no way to have a function  $u(\mathbf{r}; \mathbf{k})$  satisfying the periodicity condition  $u(\mathcal{T}_j^\pm \mathbf{r}; \mathbf{k}) = u(\mathbf{r}; \mathbf{k})$ ,  $j = \pm 1, \pm 2, \dots$ , such that  $\psi(\mathbf{r}; \mathbf{k}) = e^{i\mathbf{k} \cdot \mathbf{r}} u(\mathbf{r}; \mathbf{k})$ .

## B. Differential equation for the function $u(\mathbf{r}; \mathbf{k})$

To derive a differential equation for the function  $u(\mathbf{r}; \mathbf{k})$ , we write down the operator  $\nabla^2$  as

$$\nabla^2 = \frac{1}{r_t} \frac{\partial^2}{\partial \theta^2} + \frac{\partial^2}{\partial z^2} \quad (90)$$

and employ the representation (69) that is

$$\psi(\mathbf{r}; \mathbf{k}) = e^{i[\pi \cos(\tau - \theta) + \kappa z]} u(\mathbf{r}; \mathbf{k}). \quad (91)$$

On substituting this function into the Schrödinger equation (66) we obtain

$$\left[ -\frac{\hbar^2}{2m} \tilde{\nabla}^2 + \mathcal{V}(\mathbf{r}) \right] u(\mathbf{r}; \mathbf{k}) = \epsilon(\mathbf{k}) u(\mathbf{r}; \mathbf{k}), \quad (92)$$

where

$$\tilde{\nabla} = \frac{1}{r_t^2} \frac{\partial^2}{\partial \theta^2} + \frac{\partial^2}{\partial z^2} + \frac{2\pi i}{r_t^2} \sin(\tau - \theta) \frac{\partial}{\partial \theta}$$

$$+2i\kappa\frac{\partial}{\partial z} - \frac{\pi}{r_t^2}[i\cos(\tau-\theta) + \pi\sin^2(\tau-\theta)] - \kappa^2. \quad (93)$$

Since the function  $u(\mathbf{r}; \mathbf{k})$  possesses the symmetry property (70), it suffices to determine it within the nanotube unit cell, a single hexagon rolled around the nanotube surface.

### C. Eigenfunctions of the Hamiltonian on a SWCNT

We aim to derive a representation of eigenfunctions of the Hamiltonian on the nanotube  $\mathcal{A}(n, m)$ ,

$$\left(\frac{\hbar^2}{2m}\nabla^2 + \mathcal{V}(\mathbf{r})\right)\psi(\mathbf{r}; \mathbf{k}) = \epsilon(\mathbf{k})\psi(\mathbf{r}; \mathbf{k}), \quad (94)$$

subject to the cyclic boundary conditions

$$\begin{aligned} \mathcal{L}_{s,-L}^+ \psi(\mathbf{r}; \mathbf{k}) &= \mathcal{L}_{s,L}^+ \psi(\mathbf{r}; \mathbf{k}), \\ (\mathbf{r}; \mathbf{k}) \in \mathcal{U}_{\mathcal{A}} \times \mathcal{K}^+, \quad s &= 0, \dots, m-1, \end{aligned} \quad (95)$$

when  $1 \leq m \leq n$ , and

$$\mathcal{L}_{s,-L}^- \psi(\mathbf{r}; \mathbf{k}) = \mathcal{L}_{s,L}^- \psi(\mathbf{r}; \mathbf{k}),$$

$$(\mathbf{r}; \mathbf{k}) \in \mathcal{U}_{\mathcal{A}} \times \mathcal{K}^-, \quad s = 0, \dots, n-1, \quad (96)$$

for zigzag nanotubes,  $m = 0$ . Here,  $\mathcal{L}_{s,\pm L}^+$  and  $\mathcal{L}_{s,\pm L}^-$  are the following functionals of the boundary conditions:

$$\begin{aligned} \mathcal{L}_{s,\pm L}^+ \psi(\mathbf{r}; \mathbf{k}) &= \psi(\mathcal{T}_s^- \mathcal{T}_{\pm L}^+ \mathbf{r}; \mathbf{k}), \\ \mathcal{L}_{s,\pm L}^- \psi(\mathbf{r}; \mathbf{k}) &= \psi(\mathcal{R}_s \mathcal{T}_{\pm L}^- \mathbf{r}; \mathbf{k}). \end{aligned} \quad (97)$$

We remark that the cyclic boundary conditions (95) and (96) are SWCNTs analogues of the Born-von Karman periodic boundary conditions for flat lattices.

Analyze first chiral and armchair nanotubes. On using Theorem 1 we simplify the boundary conditions (95) as

$$e^{-iL\kappa c_+} \psi(\mathbf{r}; \mathbf{k}) = e^{iL\kappa c_+} \psi(\mathbf{r}; \mathbf{k}). \quad (98)$$

These conditions are satisfied if

$$\kappa = \kappa_\nu = \frac{\pi\nu}{Lc_+}, \quad \nu = -L, -L+1, \dots, L-1, \quad (99)$$

where  $c_+$  is the parameter defined in (42) for chiral nanotubes and  $c_+ = \frac{a}{2}$  for armchair nanotubes. For zigzag nanotubes, the boundary condition (96) yields

$$e^{iL\sqrt{3}\kappa/2} \psi(\mathbf{r}; \mathbf{k}) = e^{-iL\sqrt{3}\kappa/2} \psi(\mathbf{r}; \mathbf{k}), \quad (100)$$

and therefore

$$\kappa = \kappa_\nu = \frac{2\pi\nu}{L\sqrt{3}a}, \quad \nu = -L, -L+1, \dots, L-1. \quad (101)$$

Consider now  $4L^2$  functions  $\psi_j(\mathbf{r}; \mathbf{k}_\nu)$  given by

$$\psi_j(\mathbf{r}, \mathbf{k}_\nu) = \mathcal{T}_j^+ \psi(\mathbf{r}, \mathbf{k}_\nu) \quad (102)$$

for nanotubes  $\mathcal{A}(n, m)$ ,  $1 \leq m \leq n$ , and

$$\psi_j(\mathbf{r}, \mathbf{k}_\nu) = \mathcal{T}_j^- \psi(\mathbf{r}, \mathbf{k}_\nu) \quad (103)$$

for zigzag nanotubes  $\mathcal{A}(n, 0)$ . Here,

$$\mathbf{k}_\nu = \begin{pmatrix} -\frac{\pi}{r_t} \sin \tau \\ \frac{\pi}{r_t} \cos \tau \\ \kappa_\nu \end{pmatrix},$$

$$j = -L, \dots, L-1, \quad \nu = -L, \dots, L-1, \quad (104)$$

and  $\kappa_\nu$  is determined in (99) if  $m \geq 1$  and (101) if  $m = 0$ . Based on these functions we design representations of the eigenfunctions of the boundary value problem (94) to (96). They are

$$\Psi(\mathbf{r}; \mathbf{k}_\nu) = \sum_{j=1}^{2L} e^{-i\pi\nu j/L} \psi_j(\mathbf{r}, \mathbf{k}_\nu). \quad (105)$$

These  $2L$  functions are linearly independent, solve the wave equation (94), and satisfy the cyclic boundary conditions (95) when  $1 \leq m \leq n$  and (96) for the zigzag symmetry case,  $m = 0$ . They also obey the condition (68) of Theorem 1. Indeed, in the case  $1 \leq m \leq n$ ,

$$\begin{aligned} \mathcal{T}_l^+ \Psi(\mathbf{r}, \mathbf{k}_\nu) &= \sum_{j=-L}^{L-1} e^{-\pi i \nu j/L} \mathcal{T}_{l+j}^+ \psi(\mathbf{r}, \mathbf{k}_\nu) \\ &= \sum_{j'=l-L}^{l+L-1} e^{-\pi i \nu (j'-l)/L} \mathcal{T}_{j'}^+ \psi(\mathbf{r}, \mathbf{k}_\nu) = e^{il\kappa c_+} \Psi(\mathbf{r}, \mathbf{k}_\nu). \end{aligned} \quad (106)$$

For zigzag nanotubes, it suffices to replace in (106)  $c_+$  by  $-\sqrt{3}a/2$  and  $\mathcal{T}_l^+$  by  $\mathcal{T}_l^-$ .

Note that, as a building block, we employed the functions  $\psi_j(\mathbf{r}, \mathbf{k}_\nu)$  associated with  $s = 0$ . In the case  $m = 1$ , this is the only choice, and the number of functions used is  $2L = N$ . For zigzag and armchair nanotubes, the number of functions needed is the smallest,  $2L = N/n$ . For chiral nanotubes  $\mathcal{A}(n, m)$  ( $1 < m < n$ ), this number is  $2L = N/m$ . Since the finite number of pure rotations  $\mathcal{R}_s$  in the zigzag case and rotation-translation transformations  $\mathcal{T}_s^-$  in the case  $1 \leq m \leq n$  do not generate new linearly independent functions, the choice of functions  $\psi_j(\mathbf{r}, \mathbf{k}_\nu)$  is independent of  $s$ .

Prove finally that the eigenfunctions  $\Psi_\nu(\mathbf{r})$  are orthogonal. Let

$$\mathcal{I}_{\mu\nu} = \int_{\mathcal{A}_0} \overline{\Psi_\mu(\mathbf{r})} \Psi_\nu(\mathbf{r}) d\Omega, \quad (107)$$

where

$$\mathcal{A}_0 = \bigcup_{l=-L}^{L-1} \mathcal{U}_{\mathcal{A}}^{0l}, \quad (108)$$

and show that

$$\mathcal{I}_{\mu\nu} = 0, \quad \mu, \nu = -L, \dots, L-1, \quad \mu \neq \nu. \quad (109)$$

For the case  $1 \leq m \leq n$ , we have

$$\begin{aligned} \int_{\mathcal{A}_0} \overline{\Psi_\mu(\mathbf{r})} \Psi_\nu(\mathbf{r}) d\Omega &= \sum_{l=-L}^{L-1} \int_{\mathcal{U}_\mathcal{A}^{0l}} \overline{\Psi_\mu(\mathbf{r})} \Psi_\nu(\mathbf{r}) d\Omega \\ &= \sum_{l=-L}^{L-1} \int_{\mathcal{U}_\mathcal{A}^{00}} \overline{\Psi_\mu(\mathcal{T}_l^+ \mathbf{r})} \Psi_\nu(\mathcal{T}_l^+ \mathbf{r}) d\Omega \\ &= \int_{\mathcal{U}_\mathcal{A}^{00}} \overline{\Psi_\mu(\mathbf{r})} \Psi_\nu(\mathbf{r}) d\Omega \sum_{l=-L}^{L-1} e^{i\pi(\mu-\nu)l/L} = 0, \quad \mu \neq \nu. \end{aligned} \quad (110)$$

For the zigzag case, the derivations are similar.

## VI. TIGHT-BINDING APPROXIMATION FOR SWCNTS

Let  $\varphi_\mu(\mathbf{r})$  ( $\mu = A, B$ ) be an atomic orbital associated with one of the two carbon atoms in the unit hexagonal cell or, equivalently, the parallelogram of periods, and orthogonal to the nanotube surface. When the tube is unrolled and the surface becomes a graphene sheet, the functions  $\varphi_\mu$  are classified as  $2p_z$ -orbitals with  $z$  orthogonal to the graphene sheet. Consider a tight-binding Bloch function of a SWCNT  $\mathcal{A}(n, m)$ . For armchair and chiral nanotubes  $\mathcal{A}(n, m)$ ,  $1 \leq m \leq n$ , it has the form

$$\begin{aligned} \Phi_\mu(\mathbf{r}; \mathbf{k}_\nu) &= \frac{1}{\sqrt{N}} \sum_{s=0}^{m-1} e^{is\kappa_\nu c_-} \sum_{j=-L}^{L-1} e^{-ij\kappa_\nu c_+} \\ &\quad \times \mathcal{T}_s^- \mathcal{T}_j^+ \varphi_\mu(\mathbf{r}), \end{aligned} \quad (111)$$

where  $N = 2Lm$  and  $\nu = -L, -L+1, \dots, L-1$ . Notice that for an armchair nanotube  $c_+ = c_- = a/2$ .

For a zigzag nanotube  $\mathcal{A}(n, 0)$ , the function is introduced as

$$\Phi_\mu(\mathbf{r}; \mathbf{k}_\nu) = \frac{1}{\sqrt{N}} \sum_{j=0}^{n-1} \sum_{s=-L}^{L-1} e^{is\kappa_\nu c_-} \mathcal{R}_j \mathcal{T}_s^- \varphi_\mu(\mathbf{r}), \quad (112)$$

where  $N = 2Ln$ . It is directly verified that

$$\mathcal{T}_l^\pm \Phi_\mu(\mathbf{r}; \nu) = e^{\pm il\kappa_\nu c_-} \Phi_\mu(\mathbf{r}; \nu), \quad (113)$$

and therefore the functions (111) and (112) are Bloch functions associated with corresponding nanotubes indeed.

Following the tight-binding approximation scheme we derive the secular equation for two energy bands  $\epsilon(\mathbf{k}) = \epsilon_\pm(\mathbf{k})$

$$\begin{vmatrix} H_{AA} - \epsilon(\mathbf{k}) S_{AA} & H_{AB} - \epsilon(\mathbf{k}) S_{AB} \\ H_{BA} - \epsilon(\mathbf{k}) S_{BA} & H_{BB} - \epsilon(\mathbf{k}) S_{BB} \end{vmatrix} = 0, \quad (114)$$

where  $H = (H_{\mu'\mu})$  and  $S = (S_{\mu'\mu})$  are the Hamiltonian and overlap matrices whose entries are

$$H_{\mu'\mu} = \langle \Phi_{\mu'} | \mathcal{H} | \Phi_\mu \rangle, \quad S_{\mu'\mu} = \langle \Phi_{\mu'} | \Phi_\mu \rangle. \quad (115)$$

This brings us to the bonding  $\pi$  and antibonding  $\pi^*$  energy bands,  $\epsilon_+(\mathbf{k})$  and  $\epsilon_-(\mathbf{k})$ ,

$$\epsilon_\pm(\mathbf{k}) = \frac{-Q \pm \sqrt{Q^2 - 4|S||H|}}{2|S|}, \quad (116)$$

where we introduced the notation

$$Q = S_{AB} H_{BA} + S_{BA} H_{AB} - S_{AA} H_{BB} - S_{BB} H_{AA}. \quad (117)$$

The coefficients  $S_{\mu'\mu}$  may be expressed through integrals of the atomic orbitals over the whole nanotube surface. In the case  $1 \leq m \leq n$  they are

$$\begin{aligned} S_{\mu'\mu} &= \frac{1}{N} \sum_{s', s=0}^{m-1} e^{i(s-s')\kappa_\nu c_-} \sum_{j', j=-L}^{L-1} e^{-i(j-j')\kappa_\nu c_+} \\ &\quad \times \int \overline{\mathcal{T}_{s'}^- \mathcal{T}_{j'}^+ \varphi_{\mu'}(\mathbf{r})} \mathcal{T}_s^- \mathcal{T}_j^+ \varphi_\mu(\mathbf{r}) d\mathbf{r}. \end{aligned} \quad (118)$$

On making the substitution  $\mathbf{r}' = \mathcal{T}_{-s}^- \mathcal{T}_{-j}^+ \mathbf{r}$  we transform the coefficients to the form

$$\begin{aligned} S_{\mu'\mu} &= \frac{1}{N} \sum_{s', s=0}^{m-1} e^{i(s-s')\kappa_\nu c_-} \sum_{j', j=-L}^{L-1} e^{-i(j-j')\kappa_\nu c_+} \\ &\quad \times \int \overline{\varphi_{\mu'}(\mathcal{T}_{s'-s}^- \mathcal{T}_{j'-j}^+ \mathbf{r}')} \varphi_\mu(\mathbf{r}') d\mathbf{r}'. \end{aligned} \quad (119)$$

We next replace the indices  $s' - s = s''$  and  $j' - j = j''$  and obtain

$$\begin{aligned} S_{\mu'\mu} &= \sum_{s=0}^{m-1} e^{-is\kappa_\nu c_-} \sum_{j=-L}^{L-1} e^{ij\kappa_\nu c_+} \\ &\quad \times \int \overline{\varphi_{\mu'}(\mathcal{T}_s^- \mathcal{T}_j^+ \mathbf{r})} \varphi_\mu(\mathbf{r}) d\mathbf{r}. \end{aligned} \quad (120)$$

In the same way we transform the coefficients  $H_{\mu'\mu}$

$$\begin{aligned} H_{\mu'\mu} &= \sum_{s=0}^{m-1} e^{-is\kappa_\nu c_-} \sum_{j=-L}^{L-1} e^{ij\kappa_\nu c_+} \\ &\quad \times \int \overline{\varphi_{\mu'}(\mathcal{T}_s^- \mathcal{T}_j^+ \mathbf{r})} \mathcal{H} \varphi_\mu(\mathbf{r}) d\mathbf{r}. \end{aligned} \quad (121)$$

The entries of the Hamiltonian and overlap matrices associated with a zigzag nanotube ( $m = 0$ ) have the form

$$H_{\mu'\mu} = \sum_{j=0}^{n-1} \sum_{s=-L}^{L-1} e^{-is\kappa_\nu c_-} \int \overline{\varphi_{\mu'}(\mathcal{R}_j \mathcal{T}_s^- \mathbf{r})} \mathcal{H} \varphi_\mu(\mathbf{r}) d\mathbf{r},$$

$$S_{\mu'\mu} = \sum_{j=0}^{n-1} \sum_{s=-L}^{L-1} e^{-is\kappa_\nu c_-} \int \overline{\varphi_{\mu'}(\mathcal{R}_j \mathcal{T}_s^- \mathbf{r})} \varphi_\mu(\mathbf{r}) d\mathbf{r}. \quad (122)$$

First we restrict ourselves to the assumption that the electrons hop to the nearest atoms only. Then the diagonal  $AA$  and  $BB$  entries of the matrices  $H$  and  $S$  for any nanotube,  $0 \leq m \leq n$ , are

$$H_{\mu\mu} = \langle \varphi_\mu(\mathbf{r}) | \mathcal{H} | \varphi_\mu(\mathbf{r}) \rangle, \quad S_{\mu\mu} = \langle \varphi_\mu(\mathbf{r}) | \varphi_\mu(\mathbf{r}) \rangle.$$

The off-diagonal entries are sums of three integrals. If  $1 \leq m \leq n$ , in the sums (120) and (121) we keep the  $(s, j)$ -terms with  $(s, j)$  being  $(0, 0)$ ,  $(0, 1)$ , and  $(1, 0)$  for the entry  $H_{AB}$  and  $(0, 0)$ ,  $(0, -1)$ , and  $(-1, 0)$  for the entry  $H_{BA}$ , while discard the others. We have

$$\begin{aligned} H_{AB} &= \langle \varphi_A(\mathbf{r}) | \mathcal{H} | \varphi_B(\mathbf{r}) \rangle + e^{i\kappa_\nu c_+} \langle \varphi_A(\mathcal{T}_1^+ \mathbf{r}) | \mathcal{H} | \varphi_B(\mathbf{r}) \rangle \\ &\quad + e^{-i\kappa_\nu c_-} \langle \varphi_A(\mathcal{T}_1^- \mathbf{r}) | \mathcal{H} | \varphi_B(\mathbf{r}) \rangle, \\ H_{BA} &= \langle \varphi_B(\mathbf{r}) | \mathcal{H} | \varphi_A(\mathbf{r}) \rangle + e^{-i\kappa_\nu c_+} \langle \varphi_B(\mathcal{T}_{-1}^+ \mathbf{r}) | \mathcal{H} | \varphi_A(\mathbf{r}) \rangle \\ &\quad + e^{i\kappa_\nu c_-} \langle \varphi_B(\mathcal{T}_{-1}^- \mathbf{r}) | \mathcal{H} | \varphi_A(\mathbf{r}) \rangle. \end{aligned} \quad (123)$$

The counterparts of these formulas for a zigzag nanotube read

$$\begin{aligned} H_{AB} &= \langle \varphi_A(\mathbf{r}) | \mathcal{H} | \varphi_B(\mathbf{r}) \rangle + \langle \varphi_A(\mathcal{R}_1 \mathbf{r}) | \mathcal{H} | \varphi_B(\mathbf{r}) \rangle \\ &\quad + e^{-i\kappa_\nu c_-} \langle \varphi_A(\mathcal{T}_1^- \mathbf{r}) | \mathcal{H} | \varphi_B(\mathbf{r}) \rangle, \end{aligned}$$

with  $(j, s)$ -indices in (122) taken as  $(0, 0)$ ,  $(1, 0)$ , and  $(0, 1)$ , and

$$\begin{aligned} H_{BA} &= \langle \varphi_B(\mathbf{r}) | \mathcal{H} | \varphi_A(\mathbf{r}) \rangle + \langle \varphi_B(\mathcal{R}_{-1} \mathbf{r}) | \mathcal{H} | \varphi_A(\mathbf{r}) \rangle \\ &\quad + e^{i\kappa_\nu c_-} \langle \varphi_B(\mathcal{T}_{-1}^- \mathbf{r}) | \mathcal{H} | \varphi_A(\mathbf{r}) \rangle. \end{aligned} \quad (124)$$

with the  $(j, s)$ -indices in (122) selected as  $(0, 0)$ ,  $(-1, 0)$ , and  $(0, -1)$ , respectively. Notice that  $\kappa_\nu$  for zigzag nanotubes is defined by (101), while for the other types of nanotubes it is given by (99). The entries of the overlap matrix  $S$  are obtained from the corresponding entries of the matrix  $H$  if the Hamiltonian is replaced by the identity operator.

In the second nearest-neighbor tight-binding approximation the off-diagonal entries are not changed, while the diagonal entries gain six more terms which reflect hopping between atom  $\mu = A, B$  and the nearest atoms in the  $\mu$ -sublattice. These atoms are shown in Fig. 8 for armchair nanotubes (their location is similar in the case  $1 \leq m \leq n$ ) and in Fig. 9 for zigzag nanotubes ( $m = 0$ ). For the entry  $H_{AA}$  associated with a nanotube  $\mathcal{A}(n, m)$ ,  $1 \leq m \leq n$ , we have

$$H_{AA} = \langle \varphi_A(\mathbf{r}) | \mathcal{H} | \varphi_A(\mathbf{r}) \rangle + \langle \varphi_{A_1^+}(\mathbf{r}) | \mathcal{H} | \varphi_A(\mathbf{r}) \rangle$$

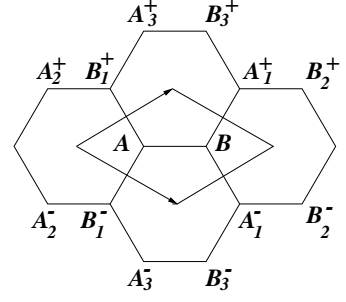


FIG. 8. Unrolled four cells of an armchair nanotube  $\mathcal{A}(n, n)$ , a parallelogram of the periods, and  $A$ - and  $B$ -sublattices.

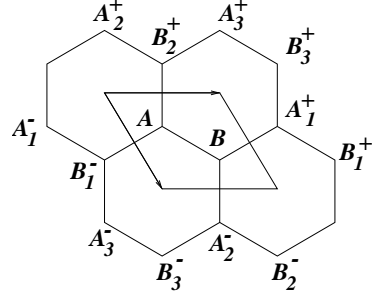


FIG. 9. Unrolled four cells of a zigzag nanotube  $\mathcal{A}(n, 0)$ , a parallelogram of the periods, and  $A$ - and  $B$ -sublattices.

$$\begin{aligned} &+ \langle \varphi_{A_1^-}(\mathbf{r}) | \mathcal{H} | \varphi_A(\mathbf{r}) \rangle + \langle \varphi_{A_2^+}(\mathbf{r}) | \mathcal{H} | \varphi_A(\mathbf{r}) \rangle \\ &+ \langle \varphi_{A_2^-}(\mathbf{r}) | \mathcal{H} | \varphi_A(\mathbf{r}) \rangle + \langle \varphi_{A_3^+}(\mathbf{r}) | \mathcal{H} | \varphi_A(\mathbf{r}) \rangle \\ &+ \langle \varphi_{A_3^-}(\mathbf{r}) | \mathcal{H} | \varphi_A(\mathbf{r}) \rangle. \end{aligned} \quad (125)$$

The  $(s, j)$ -pairs in (121) associated with the seven terms in the last relation are  $(0, 0)$ ,  $(0, 1)$ ,  $(1, 0)$ ,  $(-1, 0)$ ,  $(0, -1)$ ,  $(-1, 1)$ , and  $(1, -1)$ , respectively. Therefore

$$\begin{aligned} H_{AA} &= \langle \varphi_A(\mathbf{r}) | \mathcal{H} | \varphi_A(\mathbf{r}) \rangle + e^{i\kappa_\nu c_+} \langle \varphi_A(\mathcal{T}_1^+ \mathbf{r}) | \mathcal{H} | \varphi_A(\mathbf{r}) \rangle \\ &\quad + e^{-i\kappa_\nu c_-} \langle \varphi_A(\mathcal{T}_1^- \mathbf{r}) | \mathcal{H} | \varphi_A(\mathbf{r}) \rangle \\ &\quad + e^{i\kappa_\nu c_-} \langle \varphi_A(\mathcal{T}_{-1}^- \mathbf{r}) | \mathcal{H} | \varphi_A(\mathbf{r}) \rangle \\ &\quad + e^{-i\kappa_\nu c_+} \langle \varphi_A(\mathcal{T}_{-1}^+ \mathbf{r}) | \mathcal{H} | \varphi_A(\mathbf{r}) \rangle \\ &\quad + e^{i\kappa_\nu(c_+ + c_-)} \langle \varphi_A(\mathcal{T}_1^+ \mathcal{T}_{-1}^- \mathbf{r}) | \mathcal{H} | \varphi_A(\mathbf{r}) \rangle \\ &\quad + e^{-i\kappa_\nu(c_+ + c_-)} \langle \varphi_A(\mathcal{T}_1^- \mathcal{T}_{-1}^+ \mathbf{r}) | \mathcal{H} | \varphi_A(\mathbf{r}) \rangle. \end{aligned} \quad (126)$$

Similarly, the second diagonal entry is derived in the form

$$H_{BB} = \langle \varphi_B(\mathbf{r}) | \mathcal{H} | \varphi_B(\mathbf{r}) \rangle + e^{i\kappa_\nu c_-} \langle \varphi_B(\mathcal{T}_{-1}^- \mathbf{r}) | \mathcal{H} | \varphi_B(\mathbf{r}) \rangle$$

$$\begin{aligned}
& + e^{-i\kappa_\nu c_+} \langle \varphi_B(\mathcal{T}_{-1}^+ \mathbf{r}) | \mathcal{H} | \varphi_B(\mathbf{r}) \rangle \\
& + e^{i\kappa_\nu c_+} \langle \varphi_B(\mathcal{T}_1^+ \mathbf{r}) | \mathcal{H} | \varphi_B(\mathbf{r}) \rangle \\
& + e^{-i\kappa_\nu c_-} \langle \varphi_B(\mathcal{T}_1^- \mathbf{r}) | \mathcal{H} | \varphi_B(\mathbf{r}) \rangle \\
& + e^{i\kappa_\nu (c_+ + c_-)} \langle \varphi_B(\mathcal{T}_1^+ \mathcal{T}_{-1}^- \mathbf{r}) | \mathcal{H} | \varphi_B(\mathbf{r}) \rangle \\
& + e^{-i\kappa_\nu (c_+ + c_-)} \langle \varphi_B(\mathcal{T}_1^- \mathcal{T}_{-1}^+ \mathbf{r}) | \mathcal{H} | \varphi_B(\mathbf{r}) \rangle. \quad (127)
\end{aligned}$$

The  $AA$  and  $BB$  Hamiltonian integrals for a zigzag nanotube in the second nearest-neighbor tight-binding approximation are derived from (122). They are

$$\begin{aligned}
H_{\mu\mu} = & \langle \varphi_\mu(\mathbf{r}) | \mathcal{H} | \varphi_\mu(\mathbf{r}) \rangle + \langle \varphi_\mu(\mathcal{R}_1 \mathbf{r}) | \mathcal{H} | \varphi_\mu(\mathbf{r}) \rangle \\
& + \langle \varphi_\mu(\mathcal{R}_{-1} \mathbf{r}) | \mathcal{H} | \varphi_\mu(\mathbf{r}) \rangle + e^{i\kappa_\nu c_-} \langle \varphi_\mu(\mathcal{T}_{-1}^- \mathbf{r}) | \mathcal{H} | \varphi_\mu(\mathbf{r}) \rangle \\
& + e^{-i\kappa_\nu c_-} \langle \varphi_\mu(\mathcal{T}_1^- \mathbf{r}) | \mathcal{H} | \varphi_\mu(\mathbf{r}) \rangle \\
& + e^{i\kappa_\nu c_-} \langle \varphi_\mu(\mathcal{R}_1 \mathcal{T}_{-1}^- \mathbf{r}) | \mathcal{H} | \varphi_\mu(\mathbf{r}) \rangle \\
& + e^{-i\kappa_\nu c_-} \langle \varphi_\mu(\mathcal{R}_{-1} \mathcal{T}_1^- \mathbf{r}) | \mathcal{H} | \varphi_\mu(\mathbf{r}) \rangle, \quad \mu = A, B. \quad (128)
\end{aligned}$$

As in the first nearest-neighbor tight-binding approximation, the  $AA$  and  $BB$  entries of the overlap matrix  $S$  are found from the above formulas for the corresponding entries of the matrix  $H$  if the identity operator replaces the Hamiltonian.

We finally remark that for armchair and zigzag nanotubes, due to the symmetry, these formulas may be simplified.

## VII. CONCLUSIONS

We have proposed an analogue of the Bloch theory for a SWCNT  $(n, m)$ ,  $0 \leq m \leq n$ , whose surface is a cylindrical lattice with rotational-translational symmetry. The main difference between this theory and the conventional zone-folding technique is that it does not

entirely rely on the use of 2d characteristic vectors of the real and reciprocal hexagonal lattices of graphene. The approach proposed employs cylindrical coordinates and 3d characteristic vectors of the nanotube. It constructs a reciprocal tube that is characterized by two vectors in the 3d reciprocal space and possesses the chirality of its real counterpart. For the description of both tubes, the real one and its reciprocal, two compositions of a rotation and translation transformations were introduced. We have designed the Brillouin zone and described the domain of the wave-vector. The Brillouin zone is a nonregular hexagon rolled around the nanotube surface, while the domain for the wave-vector is a rectangle rolled around the reciprocal tube and parallel to its axis.

We have shown that the classical Bloch formula for crystals with translational symmetry,

$$\psi(\mathbf{r}; \mathbf{k}) = e^{i\mathbf{k} \cdot \mathbf{r}} u(\mathbf{r}; \mathbf{k}), \quad \mathbf{r} \in \mathcal{U}_A,$$

is also valid for SWCNTs  $(n, m)$ , 2d cylindrical lattices with rotational-translational symmetry. Here,  $\psi(\mathbf{r}; \mathbf{k})$  is a solution of the Schrödinger equation,  $u(\mathbf{r}; \mathbf{k})$  is a function invariant with respect to the composition of associated rotation-translation transformations in the real and reciprocal spaces,  $u(\mathcal{T}_j^\pm \mathbf{r}; \tilde{\mathcal{T}}_j^\pm \mathbf{k}) = u(\mathbf{r}; \mathbf{k})$ ,  $\mathbf{r} \in \mathcal{U}_A$ ,  $\mathbf{k} \in \mathcal{K}^\pm$ . Here,  $\mathcal{U}_A$  is a unit cell of the nanotube, a unit cell of graphene rolled around the nanotube surface, and  $\mathcal{K}^\pm$  are the domains of the corresponding rotation-translation transformations determined by the Brillouin zone. Based on these constructions and the tight-binding approximation scheme for an orbital orthogonal to the nanotube surface we derived the secular equation and the Hamiltonian and overlap matrices associated with the first and second nearest-neighbor approximations.

In the nearest future it is natural to proceed with computational tests and calculating the electronic structure of SWCNTs. It is of interest to develop a DFT method based on the description of the nanotube structure proposed.

## ACKNOWLEDGMENTS

This material is based upon work supported by the Office of the Under Secretary of Defense for Research and Engineering under award number FA9550-24-1-0177. The author thanks S.K. Novoselov for fruitful discussions.

---

[1] S. Iijima, Helical microtubules of graphitic carbon, *Nature*, **354**, 56-58 (1991).

[2] R. Saito, G. Dresselhaus, and M. S. Dresselhaus, *Physical Properties of Carbon Nanotubes* (Imperial College Press, London, 1998).

[3] P. R. Wallace, The band theory of graphite, *Phys. Rev.* **71**, 622-634 (1947).

[4] A. H. Castro Neto, F. Guinea, N. M. R. Peres, K. S. Novoselov and A. K. Geim, The electronic properties of graphene, *Rev. Mod. Phys.* **81**, 109-162 (2009).

[5] N. Hamada, S. Sawada and A. Oshiyama, New one-dimensional conductors: graphitic microtubules, *Phys. Rev. Lett.* **68**, 1579-1581 (1992).

[6] R. Saito, M. Fujita, G. Dresselhaus, and M. S. Dressel-

haus, Electronic structure of graphene tubules based on  $C_{60}$ , Phys. Rev. B **46**, 1804-1811 (1992).

[7] R. Saito, M. Fujita, G. Dresselhaus, and M. S. Dresselhaus, Electronic structure of chiral graphene tubules, Appl. Phys. Lett. **60**, 2204-2206 (1992).

[8] H. Ajiki and T. Ando, Electronical states of carbon nanotubes, J. Phys. Soc. Jpn **62**, 1255-1266 (1993).

[9] R. Saito, R., G. Dresselhaus, and M. S. Dresselhaus, Electronic structure of double-layer graphene tubules, J. Appl. Phys. **73**, 494-500 (1993).

[10] R.A. Jishi, D. Inomata, K. Nakao, M. S. Dresselhaus and G. Dresselhaus, Electronic and lattice properties of carbon nanotubes, J. Phys. Soc. Jpn **63**, 2252-2260 (1994).

[11] E. B. Barros, A. Jorio, G. G. Samsonidze, R. B. Capaz, A. G. Souza Filho, J. Mendez Filho, G. Dresselhaus, and M. S. Dresselhaus, Review on the symmetry-related properties of carbon nanotubes. Phys. Rep. **431**, 261-302 (2006).

[12] X. Blase, L. X. Benedict, E. L. Shirley, and S. G. Louie, Hybridization effects and metallicity in small radius carbon nanotubes, Phys. Rev. Lett. **72**, 1878-1881 (1994).

[13] A. Kleiner and S. Eggert, Band gaps of primary metallic carbon nanotubes, Phys. Rev. B **63**, 073408 (2001).

[14] V. N. Popov, Curvature effects on the structural, electronic and optical properties of isolated single-walled carbon nanotubes within a symmetry-adapted non-orthogonal tight-binding model, New J. Phys. **6**, 17 (2004).

[15] R. Barnett, E. Demler, and E. Kaxiras, Electron-phonon interaction in ultrasmall-radius carbon nanotubes, Phys. Rev. B **71**, 035429 (2005).

[16] H. M. Yu and A. S. Banerjee, Density functional theory method for twisted geometries with application to torsional deformations in group-IV nanotubes, J. Comp. Phys. **456**, 111023 (2022).

[17] S. Agarwal and A. S. Banerjee, Solution of the Schrödinger equation for quasi-one-dimensional materials using helical waves, J. Comp. Phys. **496**, 112551 (2024).

[18] F. Bloch, Über die Quantenmechanik der Elektronen in Kristallgittern. Z. f. Physik, **52**, 555-600 (1929).

[19] C. Kittel, *Quantum Theory of Solids* (John Wiley & Sons, Inc. New York, 1963).

[20] E. Kaxiras and J.D. Joannopoulos, *Quantum Theory of Materials* (Cambridge University Press, Cambridge, 2019).

[21] C. T. White, D. H. Robertson, and J. W. Mintmire, Helical and rotational symmetries of nanoscale graphitic tubules, Phys. Rev. B **47**, 5485-5488 (1993).

[22] D.-B. Zhang M. Hua and T. Dumitrica, Stability of polycrystalline and wurtzite Si nanowires via symmetry-adapted tight-binding objective molecular dynamics, J. Chem. Phys. **128**, 084104 (2008).

[23] O. O. Kit, L. Pastewka, and P. Koskinen, Revised periodic boundary conditions: Fundamentals, electrostatics, and the tight-binding approximation, Phys. Rev. B **84**, 155431 (2011).